April 2011

Energy Generation from Vortex Induced Vibrations

Aaron Scott Hall-Stinson
Worcester Polytechnic Institute

Christopher James Lehrman
Worcester Polytechnic Institute

Everett Raymond Tripp
Worcester Polytechnic Institute

ENERGY GENERATION FROM VORTEX INDUCED VIBRATIONS

BJS-VE10

A Major Qualifying Project

Submitted to the Faculty of the

WORCESTER POLYTECHNIC INSTITUTE

In partial fulfillment of the requirements for the

Degree of Bachelor of Science

By

Aaron Hall-Stinson

Christopher Lehrman

Everett Tripp

April 28, 2011

Submitted to Professor Brian J. Savilonis, Advisor

Abstract

Vortex induced vibration is a well-known fluid flow phenomenon studied in multiple engineering disciplines and typically sought to be minimized. However, a potential exists to harness this phenomenon for electrical energy generation from low velocity marine currents. In this project, a mathematical model was created to predict the dynamic response and mechanical power of elastically mounted PVC cylinders subjected to a range of flow velocities. Next, a six foot long open channel flow tank was designed and constructed to test cylinder behavior over a range of flow velocities. A total of 85 tests were conducted using five different cylinder diameters, each with several different masses, suspended on springs from a fixed apparatus submerged in the channel. Cylinder displacement, velocity, and acceleration, as well as flow velocity, were measured and recorded at a rate of 20 Hz over a one minute test interval for each trial. From these data, oscillation frequency, mean amplitude, and fluid force vs. time were calculated, as well as an estimate of available mechanical power in the cylinder oscillations. These calculations were then used with other derived properties to develop a single power coefficient curve over the range $5x10^3 < Re < 1.5x10^4$. Additionally, efficiency calculations indicated that the 0.75" cylinder had the most ideal aspect ratio of the cylinders considered. In terms of power density, the 1" cylinder produced the maximum result of $10W/m^3$.

Table of Contents

Table of Figures

List of Tables

1 Introduction

The global demand for scalable renewable energy sources is large and ever growing. Many hydrokinetic energy technologies exist currently, but are unable to truly meet this demand due to self-limitations. The Earth's water bodies constitute a huge portion of the planet and their slow and steady motion represents a vast, but as yet untapped energy resource. Most energy is currently harnessed from water flow by the joint effort of a dam and a hydroelectric generator. Newer and less ecologically intrusive technology is needed to support growing energy demand. One promising new technology that meets these criteria utilizes vortex induced vibrations in water to extract energy.

Structures subjected to fluid flow are usually designed to minimize fatigue caused by vortex induced vibrations. Only recently has the idea been proposed to enhance the vibrations in order to maximize energy extraction from the fluid. This technology works by securing a cylinder horizontally in water and constraining it to a single degree of freedom; movement up and down in the plane perpendicular to the fluid flow. Flow over this cylinder creates an alternating vortex pattern which exerts alternating lift forces on the cylinder, pushing it up and down. This motion is then converted into electricity via a power take off mechanism.

This technology is superior to traditional hydro technology in several ways. Most turbine based converters only operate efficiently at currents greater than 2 m/s, while surface oscillation converters only give high output over a small range of wave frequencies. A vortex induced vibration based generator could potentially function in slow moving waterways over a wide range of frequencies. Further, Large scale tidal and dam type systems are very capital intensive and environmentally obtrusive. The VIV concept is capable of producing energy from water flow without altering the local environment, posing any danger to nearby residents, changing the landscape in any visible way, or interfering with water traffic in any slow moving waterway (0.5-5 knots).

Energy generation from VIV has significant potential for coastal areas as well. Fifty percent of the U.S. population lives within 50 miles of the coast, whereas this coastal land accounts for only 11 percent of U.S. territory. Energy demand in these coastal regions is predictably larger than inland regions.

Scalability and versatility are two of the greatest strengths of this technology. Modules can range in size from single cylinder arrays to mega-watt producing power plants. Areas of potential power production include water bodies and/or rivers such as the Gulf Stream, the Columbia, the Missouri, the Colorado, the Mississippi, the Kansas, and the Ohio. All water bodies listed contain segments of flow averaging in the prime production speeds required for this technology, which are significantly lower than other turbine based hydrokinetic technologies.

This study examined the potential for vortex induced vibrations as a source of energy by accomplishing the following goals:

- *The development of a mathematical model to predict the dynamic response of a cylinder in water flow*
- *The design of a small-scale setup and methodology to experimentally test cylinder behavior under varying conditions*
- *The use of the experimental results to determine potential mechanical power and efficiency, and the validity of the model*
- *The use of observations and data to propose a larger scale testing setup with power take-off ability*

2 Background

In this Chapter, a qualitative as well as technical description of the vortex induced vibration phenomenon will be presented, along with relevant background on its causes and potential effects. Areas which are especially relevant to energy generation will be emphasized. The two main goals can be seen as explaining the principals of VIV, and then using those principals to create a model for energy generation which will in turn be used in designing and choosing conditions for the experimental apparatus.

2.1 VIV Theory

Vortex shedding is a widely occurring phenomenon applicable to nearly any bluff (non-streamlined) body submerged in a fluid flow. Since any real fluid flow is viscous, there will be a significant boundary layer on the bodies' surface for all but the lowest Reynolds number flows. At some point along the bodies' surface, separation of the boundary layer will occur, depending on the exact surface geometry. This separated layer, which bounds the wake and free stream, will tend to cause fluid rotation, since its outer side, in contact with the free stream, moves faster than its inner side, in contact with the wake. It is this rotation which then results in the formation of individual vortices, which are then shed from the rear of the body and travel down the wake. Typically, a pattern of periodic, alternating vortex shedding will occur in the flow behind the body, which is referred to as a vortex street. Depending on the characteristics of the flow, mainly the Reynolds number, different types of vortex streets may form, which will be discussed later in more detail.

When the pattern of shed vortices is not symmetrical about the body, which is the case in any vortex street, an irregular pressure distribution is formed on the upper and lower sides of the body, which results in a net lift force perpendicular to the flow direction. Since the vortices are shed in a periodic manner, the resulting lift forces on the body also vary periodically with time, and there for can induce oscillatory motion of the body. This occurrence alone would qualify as vortex induced vibration; however, there is a more interesting and important phenomenon, similar to linear resonance, which can occur when the frequency of vortex

shedding f_S is close to the natural frequency of the body in motion, $f_{N.}$ In this phenomenon, referred to as “lock in”, the vortex shedding frequency actually shifts to match the bodies’ natural frequency, and as a result, much larger amplitudes of vibration can occur. It is this particular aspect of vortex induced vibration, lock in, which has traditionally been of greatest concern to structural engineers, since it poses the greatest risk of damage or failure. Accordingly, the range of shedding frequencies which lock in can occur over is one of the most important research areas within vortex induced vibration, and will be discussed in more depth as it is also very relevant to the design of an energy harnessing device.

The phenomenon of vortex induced vibration is rather unique, as it is both widely known and yet still poorly understood. Historical records show that vortex shedding had been observed as early as the 15th century by da Vinci in the form of a vortex row forming behind a piling submersed in a stream (Blevins). In perhaps the first scientific analysis, Strouhal found in 1878 that the Aeolian tones caused by a wire suspended in the wind were proportional to the ratio of the wind speed to wire thickness (Blevins). In modern times, much research has been undertaken to examine both the dynamics of vortex shedding, as well as the parameters which most influence a bodies’ motion during vortex induced vibration. Although important, the details of vortex shedding itself are not as relevant to energy extraction as the flow conditions and body properties are. Therefore, more focus will be given to this later area.

From the description given earlier, it can be seen that many engineered structures which are subjected to steady fluid flow may be susceptible to vortex induced vibration. A broad range of applications, including, but certainly not limited to, offshore structures, marine risers, heat transfer equipment, mooring cables, bridges and other civil structures, nuclear reactor components, and cooling stacks are all areas where the possibility of VIV must be taken into account during the design process. Accordingly, a vast majority of the past research has focused on how to suppress vortex shedding and reduce the effects of VIV on structural motion. Despite this, the information available is still quite useful in understanding the phenomenon, and is still relevant to the topic of energy generation, where it is desired to maximize, rather than suppress VIV. As a final comment, it should be noted that much of the research encountered on VIV is still in the experimental and empirical areas, rather than analytical, and as a result it can at best be used as a guideline in the design process.

2.1.1 Vortex Shedding

Like many fluid flow phenomenon, vortex shedding has been observed to be directly dependent on the Reynolds number of the flow, which is defined in Eq. 2-1.

$$Re = \frac{UD}{\nu} \qquad \textbf{Eq. 2-1}$$

U is the free stream velocity, D is the cylinder diameter, and ν is the kinematic viscosity of the fluid. As a note, most studies in literature were in fact performed using a submerged cylinder, which is the geometry later used in the experimental methodology, so the correlation length of cylinder diameter used in Re is appropriate and widely applicable, as many submerged structures are typically cylindrical in shape.

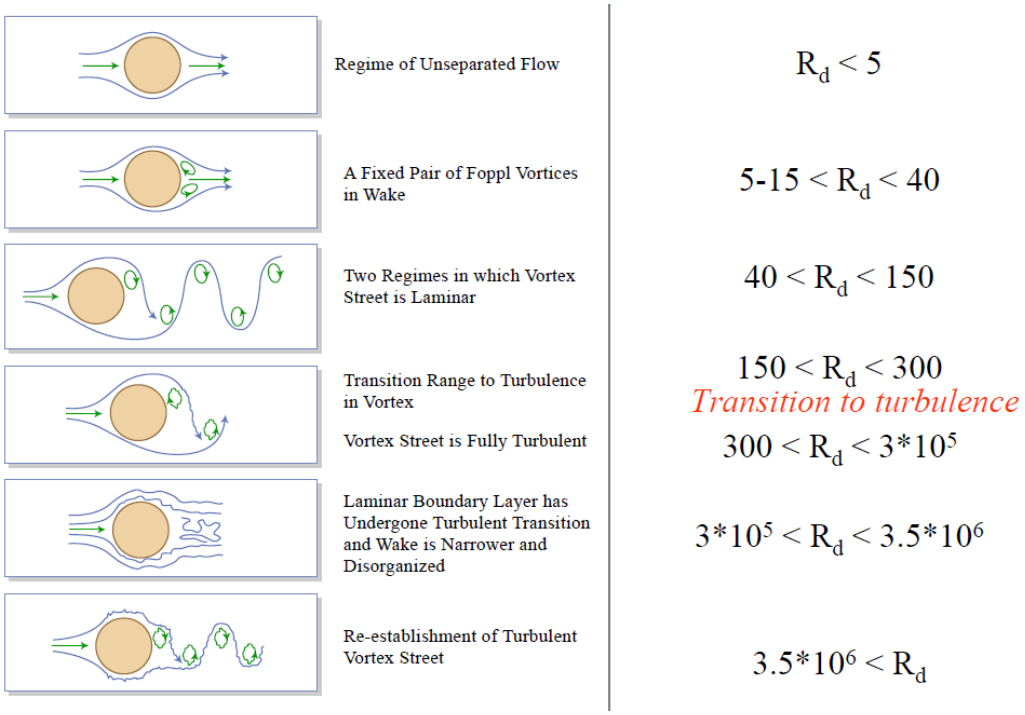

Figure 1: Vortex shedding Regimes (MIT)

The various vortex shedding patterns which occur over different ranges of Reynolds number are presented in Figure 1. For the lowest two regimes, periodic vortex shedding is nonexistent, and no resulting lift forces act on the body. For Re >40, a vortex street begins to form, which does in fact result in varying lift forces, since the vortices shed non symmetrically from the top and bottom of the cylinder. Between 150< Re<300-400, the first transition zone occurs, in which the vortex street changes from laminar flow to turbulent. As a result, no organized shedding or lift occurs in this region. For ~400<Re< $3x10^5$, the vortex street is fully turbulent, and strong, periodic shedding results (Blevins, 1990). The second transition region occurs when the flow around the cylinder changes from laminar to turbulent, and again vortex shedding is disrupted and irregular. The agreed upon ranges for this transition region were found to be varying, with the results of Lienhard giving $3x10^5$<Re< $3.5x10^6$ (Blevins), but experimental measurements by Bernitsas give the range as $3x10^5$<Re< $5x10^5$. Above this final transition region, from Re>$5x10^5$ to $3.5x10^6$, both the vortex street and cylinder boundary layer are turbulent, and regular vortex shedding resumes.

The ranges of no periodic vortex shedding, or dead zones (Bernitsas), must obviously be avoided for any device extracting energy from VIV. For the experimental system described in the methodology, the Reynolds number is on the order of the range 10^3<Re<10^4, which is well clear of both the transition zones.

2.1.2 Strouhal Number

An additional non-dimensional parameter has been established to relate the frequency of vortex shedding f_S to the flow conditions. This is given by the Strouhal number S, and is defined in Eq. 2-2.

$$S = \frac{D f_s}{U} \qquad \textbf{Eq. 2-2}$$

Again, U is the free stream velocity, and D is the cylinder diameter. For a wide range of Reynolds number, the Strouhal number varies very little, and can essentially be taken as constant, as seen in Figure 2.

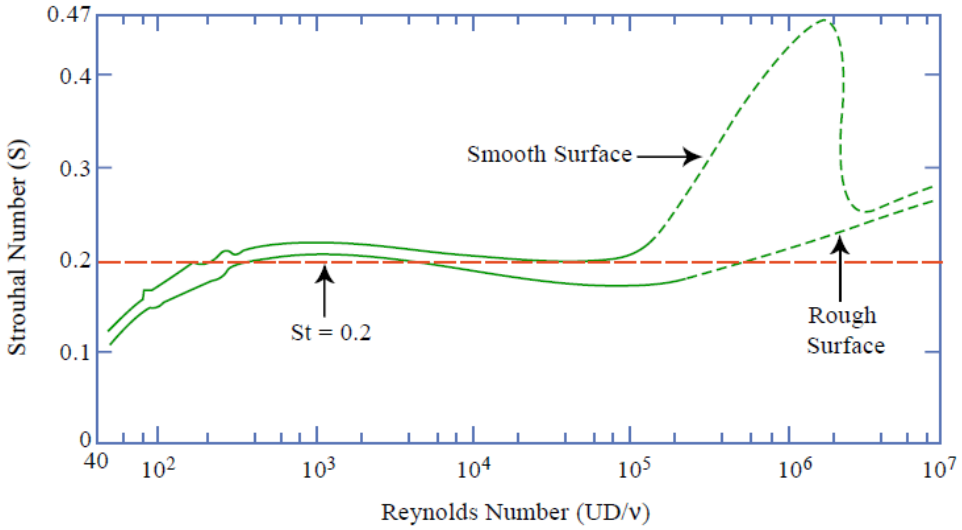

Relationship between Strouhal number and Reynolds number for circular cylinders. Data from Lienhard (1966) and Achenbach and Heinecke (1981). S~0.21 (1-21/Re) for 40<Re<200, from Roshko (1955).

Figure 2: Strouhal Number vs. Reynolds number (MIT OCW)

For the entire range of about 300<Re< 10^5, the Strouhal number is nearly 0.2 for smooth surfaces, which corresponds very well to the fully developed turbulent vortex street described earlier. Again, the range of Reynolds number considered in the experimental phase falls nearly in the middle of this constant Strouhal number region. Accordingly, S will be taken as a constant value in any experimental calculations. The result of this simplification is that the shedding frequency f_S can now be taken as dependent only on the flow velocity U for a cylinder of given diameter. For reference, the predicted shedding frequencies for the test apparatus are in the range of f_S= 0.8-2.0 s^{-1} for flow velocities between 0.15-0.30 m/s.

2.1.3 Lock In

As introduced earlier, lock in is a particular aspect of VIV which can result in relatively large amplitudes of forced vibration. An analytical theory of lock in based on first principles does not presently exist, and much of the research encountered only gives descriptive or semi-empirical evidence. As a result, the present analysis only focuses on the key findings which are relevant to achieving large amplitude vibrations, for the purpose of energy generation. Lock in is similar to linear resonance in that the vibration amplitudes increase as the natural frequency

of the cylinder is approached by the vortex shedding frequency. However, the analogy stops here, as lock in is a highly non-linear phenomenon, affected by feedback loops referred to as fluid structure interaction. Additionally, lock in does not result in the classic large amplitude spike at exactly the natural frequency, as in linear resonance. Instead, lock in has been described as both a self-limiting and self-governing occurrence, as the cylinder vibrations themselves effect the vortex shedding process, and vice versa. It is self-limiting in the sense that as the cylinder displacement increases, the vortex shedding is weakened, and hence tends to reduce further motion. Detailed experimental studies have shown that at large amplitude vibration, the vortex shedding pattern can be changed from the typical two vortices per cycle to three, as well as other unsteady combinations (Blevins).

The most important result from lock in studies has been that the phenomenon can occur over very wide ranges of shedding frequencies. This means that even at shedding frequencies significantly different than the bodies' natural frequency, the cylinder-vortex street interaction may still cause the shedding frequency to suddenly shift, matching the natural frequency, and causing powerful, large amplitude vibrations. The non-dimensional parameter used in many experiments measuring vibration amplitude is the reduced velocity U*, given by Eq. 2-3.

$$U^* = \frac{U}{f_n D} \qquad \textbf{Eq. 2-3}$$

For values of shedding frequency near the bodies' natural frequency, the Strouhal relation can be used to show that U* has the value of 1/S, or about 5. Using this as a reference point, experimental data has shown that lock in occurs for values of 3< U*<8 (Blevins), which means that shedding frequencies within a range of about +/- 30% of the natural frequency can lock on and shift to match the natural frequency.

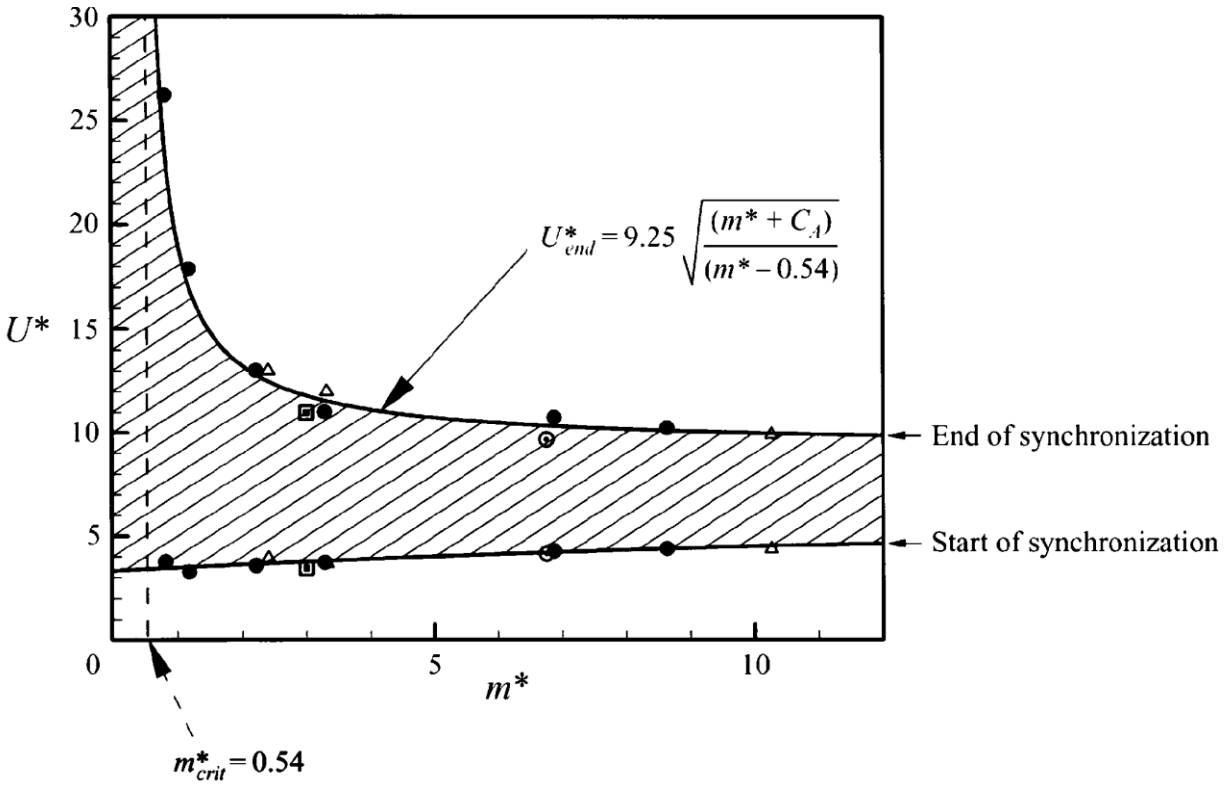

Figure 3: Reduced Velocity vs. Mass Ratio (Williamson and Govardhan)

To further complicate things, studies reviewed by (Govardhan, 2004) have shown that the range over which lock in occurs has a strong dependence on another non-dimensional parameter, the mass ratio m*, defined as m_{osc}/m_d, where m_d is the displaced fluid mass, or simply the cylinder volume multiplied by the fluid density. For large values of m*, the lock in range does not vary significantly as the oscillating mass is changed. However, as seen in Figure 3, as the value of m* approaches 2, the upper limit of the lock in range begins to grow exponentially.

By extrapolating the data outward, it was found that at a mass ratio of 0.54, the lock in region extended to infinity on the upper side, suggesting that this value was a type of "critical mass" for VIV (Govardhan, 2004). This phenomenon has also been taken into consideration for the test apparatus, as the mass ratio m* for the considered 1.25" PVC cylinder has been calculated as ~0.46. However, it is unknown if this will have the desired effect of expanding the lock in region, as it is additionally noted that this phenomenon is only applicable to systems of low reduced mass-damping product, given by the criteria $(m^* + 1)\zeta < 0.05$. The damping

considered for the test apparatus may meet this criterion; however, much greater damping will need to be added for the implementation of a power take off system, and will definitely be well above ζ=0.03, which is the limit for satisfying the criterion.

2.1.4 Boundary Gap

Another modeling constraint affecting the oscillation of the cylinder is the boundary gap ratio. The gap ratio is equal to the minimum distance between the cylinder and lower flow surface boundary divided by the diameter of the cylinder. (Raghavan, Bernitsas, & Maroulis, 2009) demonstrated that the coefficient of viscous drag and lift coefficient were directly related to the gap ratio. As the gap ratio increases, viscous drag decreases and lift increases. This is due to the effect of the gap ratio on vortex shedding. When the cylinder is in close proximity to the flow surface boundary, flow over the cylinder is uneven. Normal vortex shedding patterns are weakened or disrupted completely. It was found that, for a boundary gap value of about 3.0 or greater, the effect of the boundary gap on vortex shedding was negligible. To calculate an appropriate gap distance for a 1.25” diameter cylinder, as will be used in the test apparatus, multiply the cylinder diameter by three: 3*1.25” = 3.75”. This yields a gap ratio of 3, rendering the effects of the boundary on vortex shedding negligible.

2.2 VIVACE

The Vortex Induced Vibration Aquatic Clean Energy converter design was patented in 2008 by Professor Michael Bernitsas of the University of Michigan. The converter harnesses energy from water flow using vortex induced vibrations.

The VIVACE system is composed of a cylinder secured horizontally in a stationary frame and allowed to oscillate transverse to the direction of water flow. The cylinder is connected to the frame at the ends of the cylinder, where magnetic sliders move up and down over a rail containing a coil. The motion of the magnet over the coil creates a DC current, which can be stored or converted to AC to be sent into the grid.

This technology is superior to dam technology in several ways. It is capable of producing energy from fluid flow without altering the local environment, posing any danger to nearby residents, changing the landscape in any visible way, or interfering with water traffic in any slow moving waterway (0.5-5 knots). Energy generation from VIV has significant potential for coastal areas as well. Fifty percent of the U.S. population lives within 50 miles of the coast, whereas this coastal land accounts for only 11 percent of U.S. territory. Energy demand in coastal regions is much larger than demand inland.

Scalability and versatility are two of the greatest strengths of this technology. Modules can range in size from single-cylinder arrays to thousand-cylinder, mega-watt producing power plants. In their initial report, Bernitsas et al. outline array specifications for 1kW to 1000MW cylinder arrays. Areas of potential power production include ocean water bodies and rivers. Flow in the prime production speeds required for this technology is significantly lower than for other turbine based hydrokinetic technologies.

According to Bernitsas, VIVACE has superior energy density compared with other non-turbine ocean energy technologies. As of August 2010, Bernitsas' start-up company, Vortex Hydro Energy, has begun open water tests in the St. Clair River in Port Huron, MI.

3 Modeling

In order to establish estimates of the potential dynamic performance of a VIV based energy harnessing device, a relatively simple mathematical model was constructed to describe the fluid-oscillator interaction. This section seeks to explain this process and also demonstrate the results for one particular cylinder size. Since a basic concept of how the testing would later be carried out had already been established, many physical parameters of the setup were known or at least bounded within a specific range. The initial model calculations were based on the use of a 1.25 in nominal diameter PVC pipe section, and the geometrical and fluid properties show in Table 1.

Property	Variable	Value
Cylinder diameter	D	0.042 m
Cylinder length	L	0.22 m
Linear cylinder density	ρ_{cyl}	0.64 kg/m
Water density	ρ_{fluid}	998 kg/m^3
Water kinematic viscosity	v	1.31E-6 m^2/s
Maximum flow speed	U	0.35 m/s

Table 1: Cylinder and Flow Parameters

All fluid properties were taken at 20°C, sine the experiments were carried out at room temperature. Although the flow velocity was one of the main variables under control during the experimental phase, the maximum value achieved was used here to establish upper limits on performance. Eq. 3-1 below shows the value of the Reynolds number based on initial parameters.

$$Re = \frac{UD}{v} = 1.122 * 10^4 \qquad \textbf{Eq. 3-1}$$

For 300<*Re*< 3x10^5, the vortex street behind the cylinder is known to be fully turbulent, and strong, periodic shedding results. Accordingly, for a fixed pipe size, a wide range of flow velocities are possible while still resulting in a suitable value of Reynolds number for vortex shedding to occur.

The Strouhal number determines the vortex shedding frequency as an empirical function of *Re* over a wide range of flow speeds (Eq. 3-2).

$$S = 0.198\left(1 - \frac{19.7}{Re}\right) = 0.198 \quad \textbf{Eq. 3-2}$$

The Strouhal number is insensitive to Reynolds number and thus flow speed, as *S* remains nearly constant for 10^3<*Re*<10^5. For this reason, the *S* will be treated as a constant throughout the experiment. The vortex shedding frequency f_S is then calculated from Eq. 3-3.

$$f_s = \frac{SU}{D} = 1.647\frac{1}{s} \quad \textbf{Eq. 3-3}$$

This will be the main variable of interest for achieving large amplitude vibrations, since it must be matched to the natural vibration frequency of the cylinder in order to achieve large amplitude vibrations.

In the experiments, the vortex shedding frequency will be determined by the flow conditions and cylinder size. To match the cylinder's natural frequency to the vortex shedding frequency, the following cylinder properties were determined.

$$Vol = \frac{\pi}{4} * D^2 * L \quad \textbf{Eq. 3-4}$$

$$m_{dis} = \rho_{fluid} * Vol = 0.277kg \quad \textbf{Eq. 3-5}$$

$$m_{add} = 0.0kg \quad \textbf{Eq. 3-6}$$

$$m_{pipe} = \rho_{cyl} * L + m_{add} = 0.128kg \quad \textbf{Eq. 3-7}$$

$$m_{app} = m_{pipe} + m_{dis} = 0.405kg \quad \textbf{Eq. 3-8}$$

Mass m_{add} (Eq. 3-6) represents additional mass added to the pipe, which will initially be set as 0. The pipe mass m_{pipe} (Eq. 3-7) was determined based on unit length density of 0.64kg/m. The term m_{dis} (Eq. 3-5) represents the mass of fluid displaced by the cylinder, and must be added to take into account the force which must be exerted as the cylinder pushes the fluid out of its path. The apparent mass of the pipe in the fluid is then given by Eq. 3-8 as the sum of the pipe mass and displaced fluid mass. It is this value of apparent mass which should

then be used to determine the natural frequency of the cylinder in water. The natural frequency of vibration is determined in Eq. 3-9.

$$\omega_n = \sqrt{\frac{k}{m_{app}}} = 9.94 \frac{rad}{s} \quad \textbf{Eq. 3-9}$$

For this particular system, *k* represents the stiffness of the springs used to suspend the pipe, which will be controlled approximately to 0.2 lbf/in. This value of *k* was chosen to match the natural frequency to the shedding frequency. For these chosen values, the frequency ratio *f** is equal to 1.041, which is well within the ± 30% lock-in range.

The motion of the cylinder was modeled by a general equation of motion for linear vibration (Eq. 3-10).

$$my" + 2m\zeta\omega_n y' + ky = F(t) \quad \textbf{Eq. 3-10}$$

This model is only an approximation due to the non-linear nature of vortex shedding; however, experimental studies have shown that this approximation is accurate. This equation includes the term *m*y''* representing the inertia of the cylinder, $2m\zeta\omega_n y'$ representing the viscous drag force (damping), and the restoring force *k*y*. A value of 0.06 is assumed for ζ based on experimental findings of similar vortex induced vibration studies. *F(t)* represents the periodic force exerted on the cylinder by the vortices. In this model, *F(t)* is assumed to be a sinusoidal function with frequency equivalent to natural frequency of the cylinder, representing the condition of lock-in. The equation for F_L (Eq. 3-11) comes from the definition of lift force and gives the amplitude of *F(t)*.

$$F_L = \frac{1}{2}\rho_{fluid} U^3 D L C_L = 0.309N \quad \textbf{Eq. 3-11}$$

Coefficient of lift C_L is assumed to be 0.6 as a conservative estimate based on background research. Realistically, C_L varies with displacement of the cylinder, so this value is an average. The solution for the amplitude of the cylinder vs. time is given by Eq. 3-12. Figure 4 shows cylinder amplitude in terms of cylinder diameter as a function of time.

$$y_{res}(t) = \frac{F_L * sin\left(\omega_n t + \frac{\pi}{2}\right)}{k\sqrt{\left(1 - \left(\frac{f_s}{f_n}\right)^2\right)^2 + 4\zeta^2\left(\frac{f_s}{f_n}\right)^2}}$$ **Eq. 3-12**

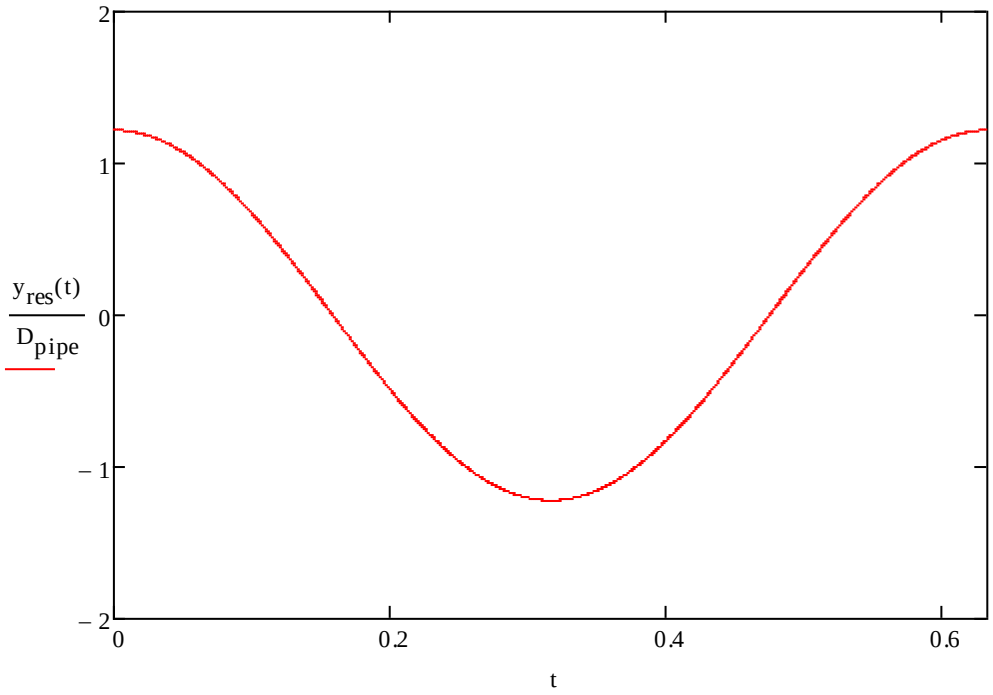

Figure 4: Cylinder Amplitude over Diameter as a Function of Time

Velocity of the cylinder is found by differentiating the equation for displacement with respect to time (Eq. 3-13), and is shown in Figure 5.

$$v(t) = \frac{d}{dt} y_{res}(t)$$ **Eq. 3-13**

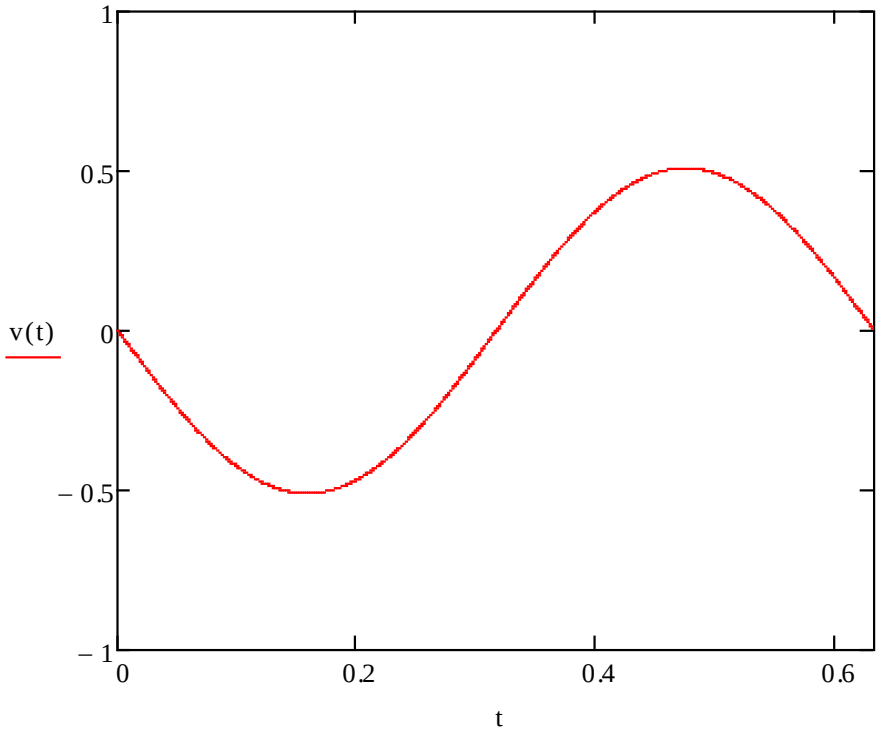

Figure 5: Derived Cylinder Velocity

Maximum velocity of the cylinder is about 0.5 m/s at the point where cylinder displacement is zero.

Power is determined by the product of the velocity and force of lift exerted on the cylinder by vortex shedding (Eq. 3-14). As seen in Figure 6, the frequency of *P(t)* is twice the frequency of either *v(t)* or F_L since it contains the product of sine and cosine.

$$P(t) = v(t) * F_L * sin(\omega_n t) \qquad \textbf{Eq. 3-14}$$

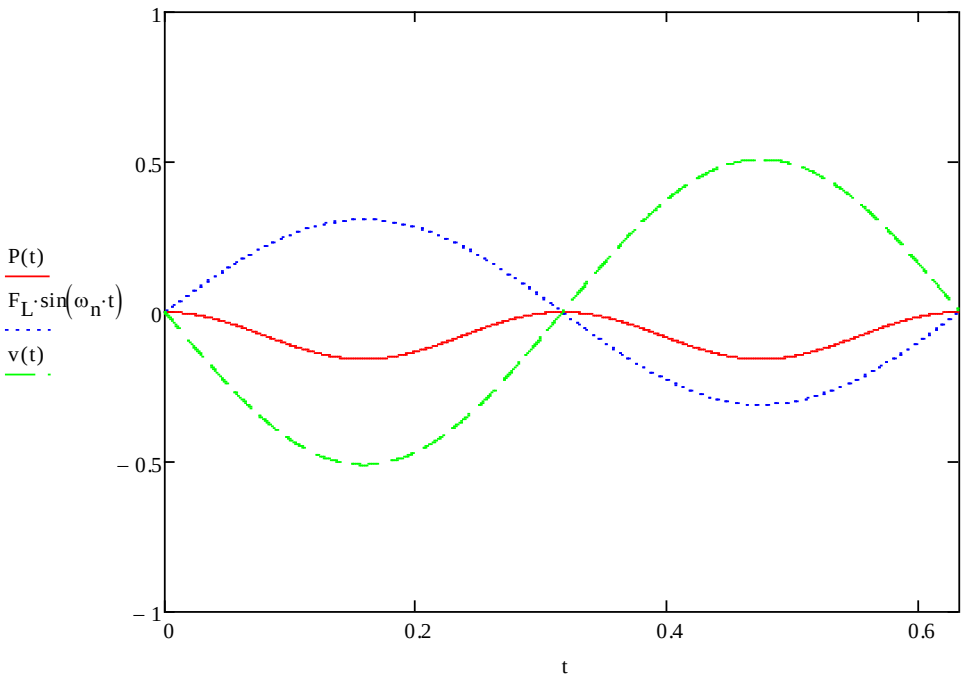

Figure 6: Cylinder Power with Defining Parameters

Maximum power amplitude is calculated to be 0.063W. Average power for the cylinder is determined in Eq. 3-15. The theoretical upper limit of power in the fluid is represented by Eq. 3-16.

$$P_{RMS} = \frac{P_{max}}{\sqrt{2}} = 0.045W \qquad \textbf{Eq. 3-15}$$

$$P_{fluid} = \frac{1}{2}\rho_{fluid} * U^3 * D * L = 0.18W \qquad \textbf{Eq. 3-16}$$

Eq. 3-16 is derived from the product of force exerted on the cylinder by fluid flow and flow velocity. Efficiency η is calculated to be:

$$\eta = \frac{P_{RMS}}{P_{fluid}} = 0.247 \qquad \textbf{Eq. 3-17}$$

This efficiency falls within the range shown in VIVACE studies, although VIVACE power output was much larger.

4 Methodology

This section discusses the physical set up of the flow tank and all components. A design process is discussed, including the reasoning behind selection of the tank design and sensor type. The experimental progression followed throughout this project is outlined.

4.1 Experimental Setup

In order to test the VIV phenomenon, an open channel flow tank was needed. Sump pumps were researched based on pumping capacity and price. From our initial calculations, a flow speed of 0.35 m/s through the channel area matched the Reynolds number range we wanted (Re = 300 to $3*10^5$), and was calculated to require a volumetric flow rate of 30,920 gallons per hour (GPH). It was later found using a flow rate sensor that the recirculating nature of the tank allowed channel flow speeds of up to 0.32 m/s with a total of only 9,130 GPH total pump capacity.

The objective of the tank design was to provide a uniform and steady flow speed within a data collection area. The initial tank design was for a circular flow tank of 4' diameter, but at the expected flow speeds it was anticipated that uneven flow velocity across a channel cross section due to the curve of the tank would be problematic. The final recirculating tank design was reached, which eliminated these problems, and provided a consistent flow through the test area.

To measure the energy flow rate of the cylinder during vibration, it was necessary to measure the acceleration and displacement of the cylinder in the water, as well as flow velocity. Measurement systems that would work under water were initially considered. A linear slider pushed by the cylinder to the distance of its maximum amplitude was initially considered; that method recorded only maximum amplitude, not amplitude over time. Laser Doppler velocimetry was researched for the purpose of measuring flow velocity and flow patterns, but required the use of a dye in the water to make readings. It was found through testing that dye in the moving water dispersed within a matter of a few seconds and the water color quickly became uniform. The technology was also found to be too expensive. The final set up involved

the measurement of movement of an out of water platform supported over the cylinder using a sonic motion sensor, and use of propeller type flow sensor placed in the central channel.

4.1.1 Materials

The following materials and equipment were used in the set up.

1. 6'x2'x2' water tank
2. 5 gallon bucket
3. Schedule 40 PVC pipe, 0.75"-2.0" diameter
4. 3125 GPH sump pump (2)
5. 2880 GPH sump pump
6. 0.75"x16"x48" boards (3)
7. Aluminum stock
8. Extension spring (4)
9. Vernier Flow Rate Sensor
10. Vernier MD BTD (Displacement Sensor)
11. Vernier LabPro
12. Logger Pro Computer Software

4.1.2 Description

The experimental set-up was assembled within a 6'x2'x2' water tank using. Data was collected within a central channel 4' long by 11¾" wide placed in the center of the tank. Figure 7 and Figure 8 show the channel within the tank.

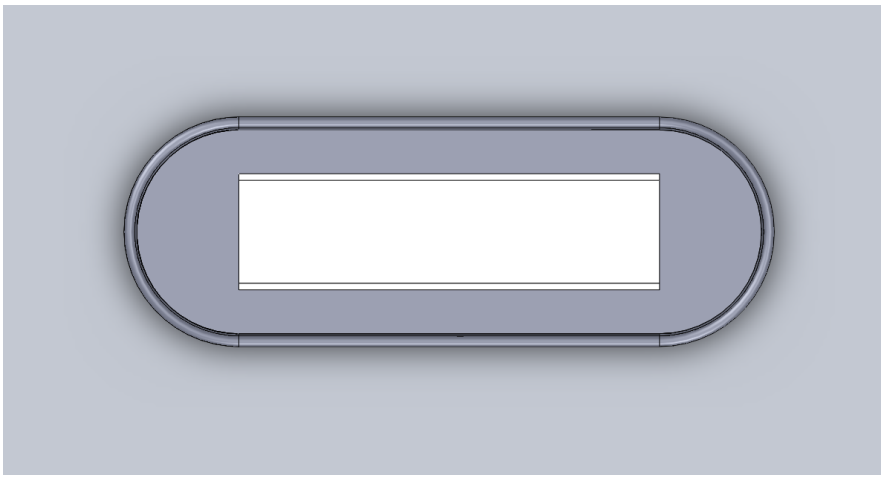

Figure 7: Tank and Channel Top View

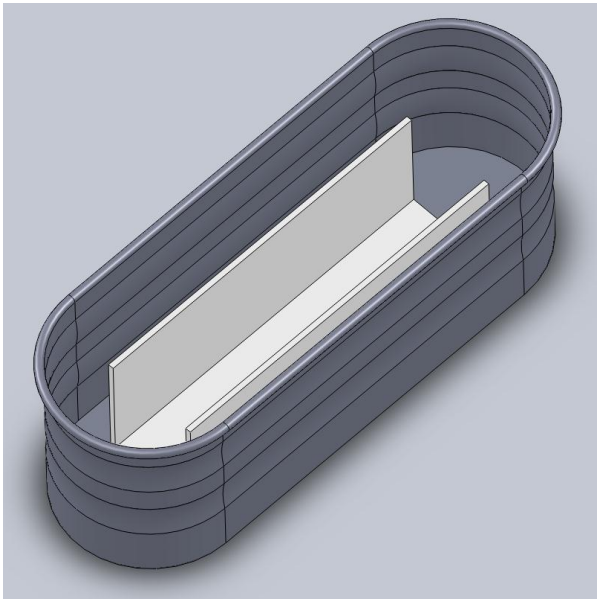

Figure 8: Tank and Channel Isometric View

On one end of the tank, sump pumps drew in water and pumped it towards the other end via the two thin channels created between the walls of the central channel and the walls of the tank. The two side pumps were rated at 3125 GPH each and the central pump was rated at 2880 GPH. The piping used for the pumps was 1.25” diameter schedule 40 PVC pipe and pipe components. For each of the two side pumps, a threaded connector, an elbow, and a 16” length of straight pipe were used. For the central pump, a threaded connector, a ball valve, a T split, two 7” lengths, two elbows, and two 16” lengths were used. The valve allowed adjustment of the flow velocity during testing.

On the other end of the tank, two flow guides served to merge flow from the side channels and direct it through the central channel. The purpose of the flow guides was to redirect flow in the smoothest manner possible. Since the test channel was short, it was important to smooth the flow as much as possible before it reached the cylinder testing area. Figure 9 and Figure 10 show the tank with pumps, Figure 11 illustrates the flow guides, and Figure 12 shows the complete assembly.

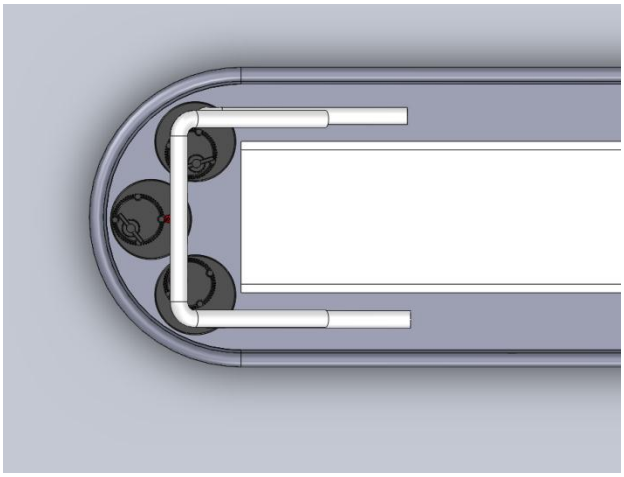

Figure 9: Pumps Top View

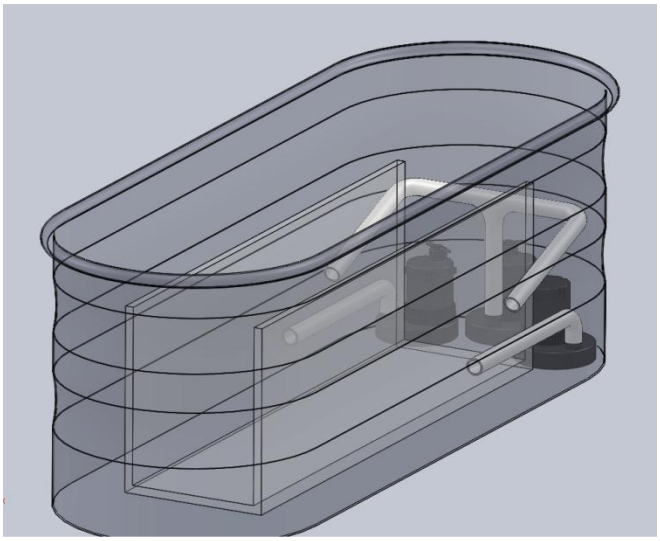

Figure 10: Pumps Isometric View

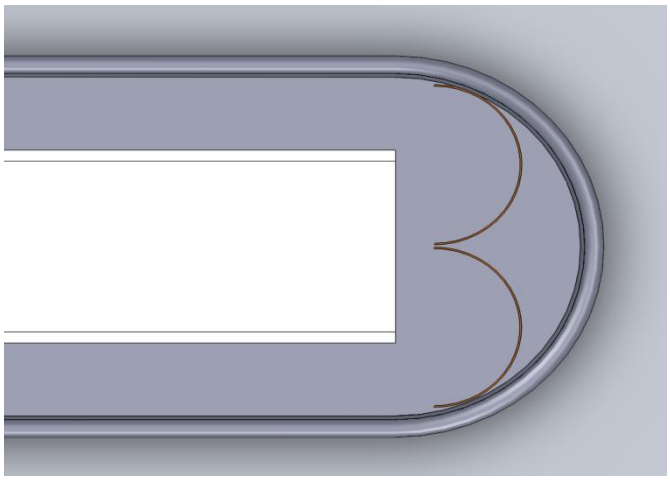

Figure 11: Flow Guides Top View

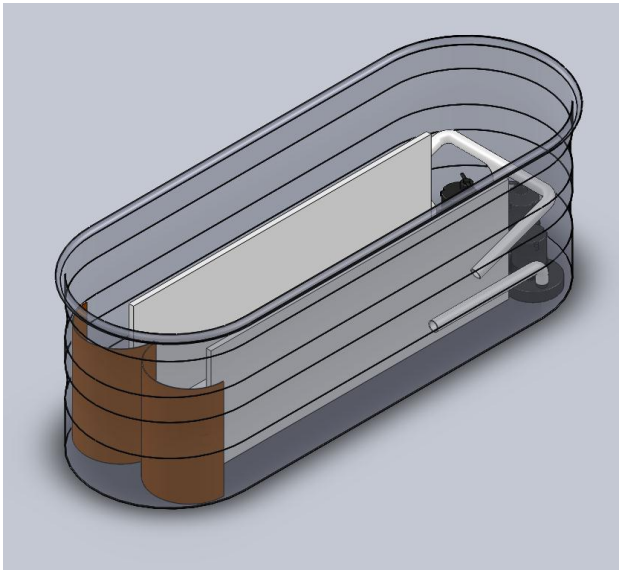

Figure 12: Tank with Pumps and Flow Guides

Initially, walls were placed in the side channels with holes fit to and secured around the sump pump pipes in order to block any flow unless pumped through the pipes. These were intended to prevent flow from pumps returning directly back to the pump inlet without first circulating through the center channel, but they were found to restrict tank flow and decrease overall flow speed.

Five cylinders of varying diameter were constructed from PVC schedule 40 piping. All cylinders were approximately nine inches in total length, with ¾”, 1”, 1 ¼”, 1 ½”, and 2” nominal diameters. The true outer diameters of these cylinders were 1.050”, 1.315”, 1.660”, 1.900”, and 2.375” respectively. Stock PVC end caps were pressed onto the ends of the cylinders to seal

them. A small hole was drilled into each cylinder, equidistant from the ends, where the measurement platform apparatus was connected. The measurement platform apparatus consisted of a thin wooden dowel approximately eight inches in length, with a small thin metal square on one end. The mass of the platform was 4 grams. This apparatus was designed to provide a dry platform from which to measure the displacement, velocity, and acceleration of the cylinder while the cylinder was submerged. Figure 13 shows the different size cylinders and Figure 14 shows the 1.25" cylinder with platform. Table 2 shows final cylinder mass for each diameter.

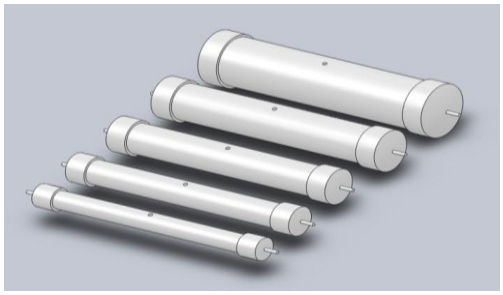

Figure 13: Cylinder Diameters

Table 2: Cylinder Mass by Diameter

0.75"	**104g**
1.00"	158g
1.25"	194g
1.50"	272g
2.00"	337g

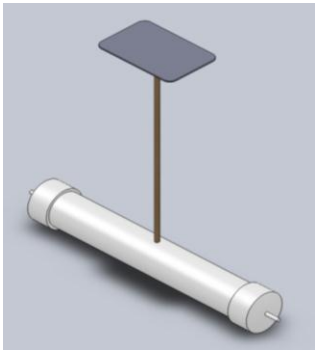

Figure 14: Cylinder with Platform Apparatus

Holes were drilled into the end caps oriented concentric to the cylinder pipe. Pre-cut wooden dowels were inserted into the end cap holes to provide a location about which to wrap the ends of the springs. Two or four springs were used, with one or two on each side in parallel to each other. These springs were attached at the other ends to the cylinder housing. Springs were selected based on calculations from the mathematical model. In order to achieve lock-in range, for cylinders of the given mass and given flow speed, total spring stiffness needed to be close to 46N. Springs used in the final set up had a stiffness of 12N each, for a total stiffness of 48N.

The cylinder housing was constructed to rest upon the channel walls at any location within the channel. The housing consisted of an aluminum top plate, 12”x8”, with an 8” by 5” rectangle cut out to allow for cylinder visibility and space for the measurement platform to oscillate. This plate lay flat on top of the channel walls. Two more aluminum plates extended from this plate into the water in the channel, connected by L-brackets, and oriented perpendicular to the top plate and parallel to the channel walls. Holes were drilled in each of the side plates one inch below the top plate, and every half inch thereafter for four inches in order to allow for adjustability of the two top screws. The cylinder housing is shown in Figure 15.

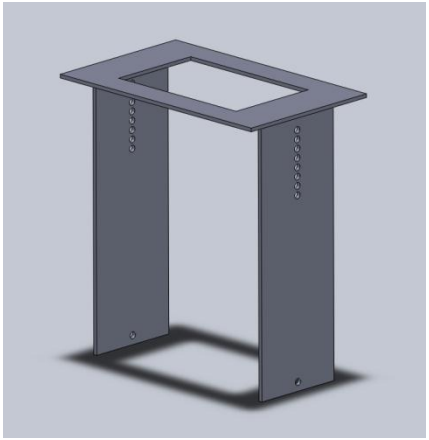

Figure 15: Cylinder Housing

The top holes were drilled to allow adjustments in the position of the top screws. One bottom hole was drilled in each side plate for the bottom screws, such that the distance from the holes to the channel bottom was one inch. The screws in the side plates provided the

second point of attachment for the four springs. The cylinder and springs were oriented in this housing such that the five parts (four springs and one cylinder at a time) created an “H” shape, with the cylinder oriented horizontally. This arrangement is shown from the front view in Figure 16, the isometric view in Figure 17, and the arrangement as placed in the channel is shown in Figure 18.

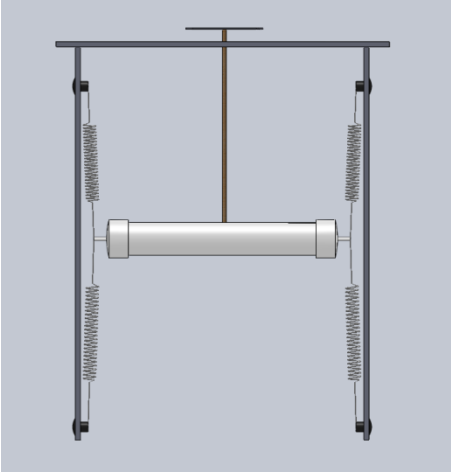

Figure 16: Cylinder Arrangement Front View

Figure 17: Cylinder Arrangement Isometric View

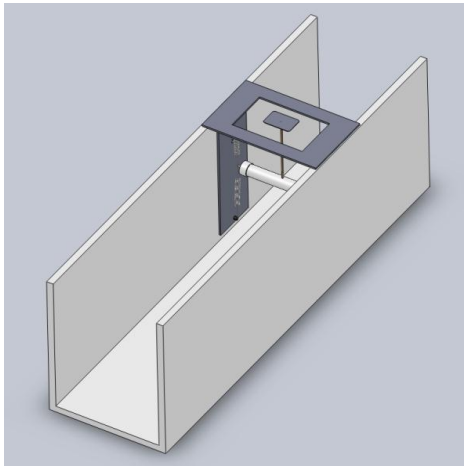

Figure 18: Cylinder Arrangement in Channel

Two nails were inserted into the inner channel walls near the inlet, one on each side. A three foot length of thin metal wire was tied to each nail. The wires ran along the channel walls and attached at the other end to the wooden dowels protruding from the cylinder end caps. These wires restricted the cylinder from moving downstream within the channel, and limited its motion to a nearly vertical direction. The proper placement of the cylinder housing in the channel was determined from the wire connection by noting the point at which the springs appeared to be closest to vertical when the water was flowing. The full tank set up is shown in Figure 19.

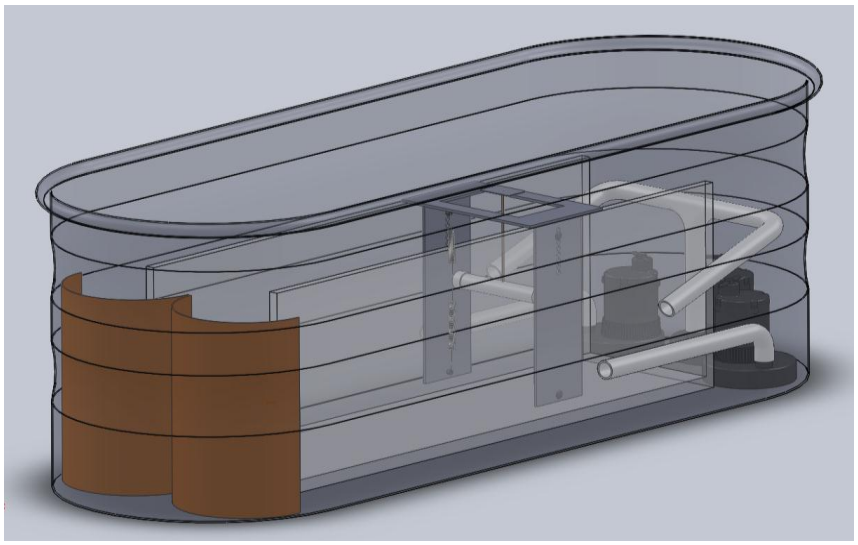

Figure 19: Test Set Up

Data was taken with two Vernier instruments, the Vernier Flow Rate Sensor and the Vernier MD BTD (Displacement Sensor). The MD BTD recorded displacement data from the dry oscillating platform supported over the cylinder, from which the computer software (Logger Pro 3) extrapolated velocity and acceleration data. The propeller type Flow Rate Sensor had a three inch diameter rotor and allowed us to measure flow in any small section of the tank. To create a flow velocity profile of the channel, flow rate was measured at three channel heights at five locations in the channel moving from right to left. The MD BTD is shown in Figure 20 (left) along with the Flow Rate Sensor (right), and the two devices are shown in approximate measurement positions within the tank in top view (Figure 21) and isometric view (Figure 22 and Figure 23).

Figure 20: Vernier MD BTD Sensor and Flow Rate Sensor

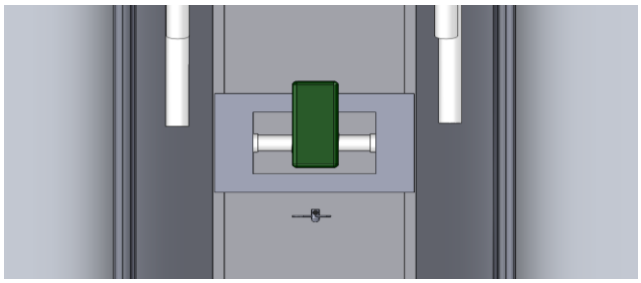

Figure 21: Measurement Location Top View

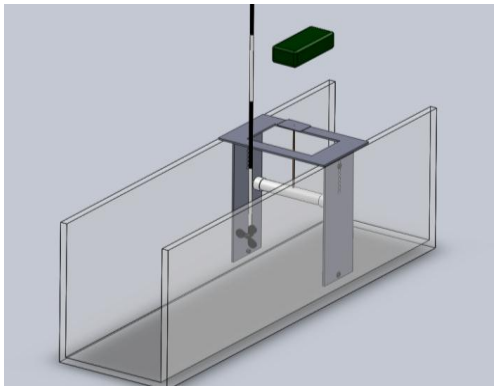

Figure 22: Measurement Location Isometric View

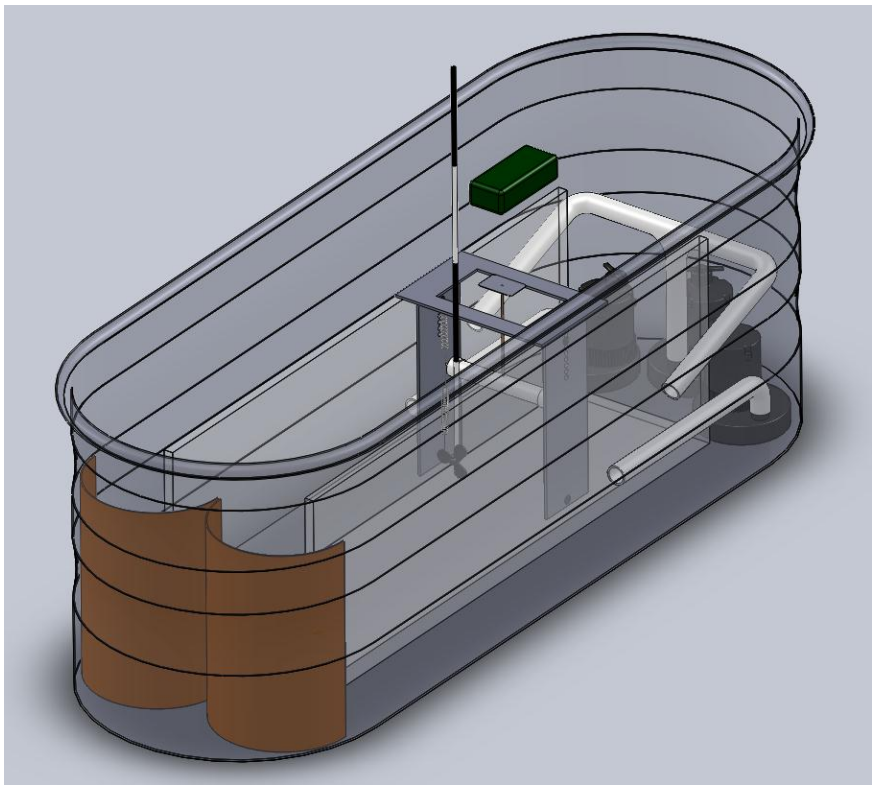

Figure 23: Final Set-Up

4.2 Experimental Procedure

To compare the response of the physical system to that of the mathematical model, a number of parameters needed to be determined experimentally. Displacement, velocity, and acceleration were measured directly using the motion sensor. Flow velocity was measured using the impeller flow sensor. Mass was measured using an electronic scale, and diameter of the cylinders was measured with calipers. All other data from experiments was derived directly or indirectly from these measured values. The relationships between the measured and derived variables are discussed with more depth in the Analysis chapter of this report.

The mathematical model assumed a steady flow profile across the entire length of the cylinder. Once the flow tank had been constructed, the validity of this assumption was tested experimentally. The differential equation for the response of the system includes variables of spring stiffness, damped natural frequency, and the damping ratio. These values were determined experimentally as explained below. The displacement, velocity, and acceleration of cylinders subjected to fluid flow were measured using the motion sensor.

4.2.1 Data Collection

The Vernier MD-BTD Motion Detector 2 measures the position of objects with the use of ultrasound waves. The detector has a range of 0.15m to 6m and a resolution of 1mm. The detector can be zeroed based on the neutral position of a stationary object. The maximum sampling rate is 50Hz.

The Vernier FLO-BTA Flow Rate Sensor measures the velocity of flowing water. The sensor consists of an impeller. The rotational speed of the impeller is proportional to the speed of the flowing water. A magnet in the impeller triggers a switch with each half rotation. The switch creates a pulse that the signal conditioner then converts to a voltage that is proportional to the flow velocity. This device is pre-calibrated by the manufacturer. The sensor has a range of 0 to 5 m/s, a resolution of 0.0012m/s, and a response time of 98% of full scale reading in 5s.

The Vernier LabPro is a data collection interface that is compatible with both the motion detector and the flow rate sensor. The Motion Detector connects to a digital input of the LabPro device. The Flow Rate Sensor connects to an analog input of the LabPro device. When

LabPro is connected to a computer through a USB cable, it works in conjunction with the LoggerPro computer software. The device automatically detects the sensors currently connected and creates the appropriate interface with the software. This allowed data for both flow velocity and cylinder displacement to be measured and displayed simultaneously. Recording of data begins and ends by pressing collect. A sampling rate and sampling time can be defined by the user. The raw data from the experiment can be imported to an excel spreadsheet with the appropriate headers for each data type intact. The LoggerPro interface used for the experiment is shown in Figure 24.

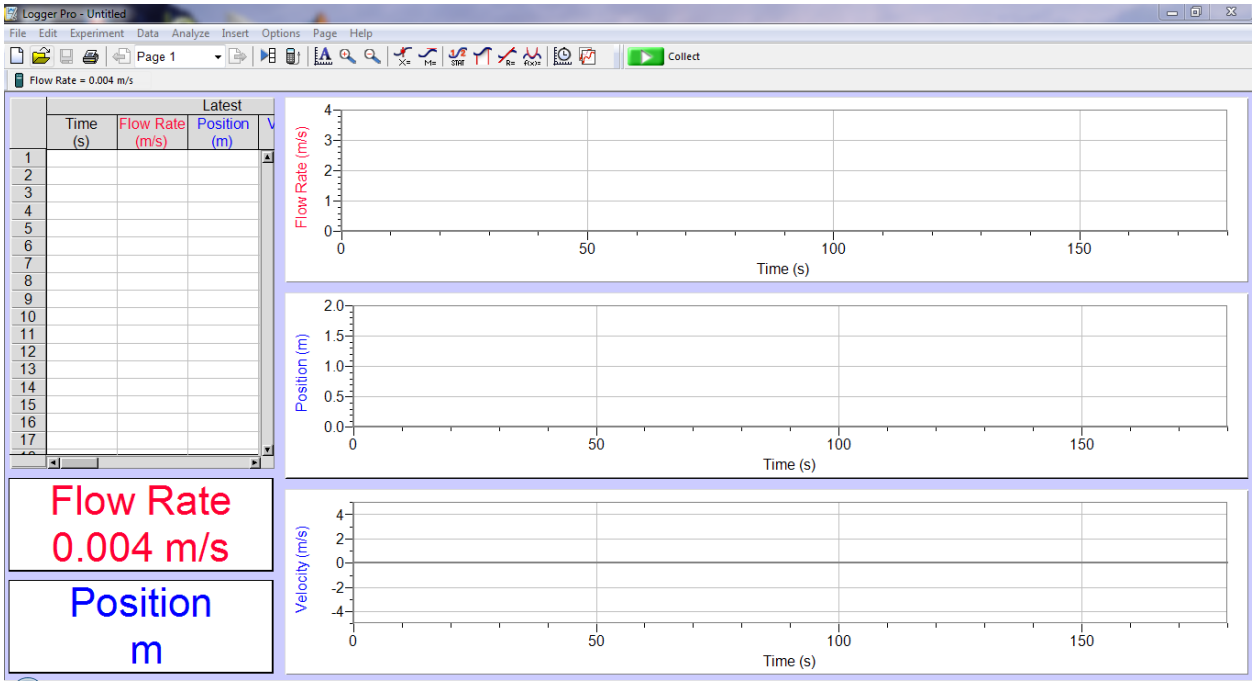

Figure 24: The LoggerPro Interface

4.2.2 Flow Profile Measurements

1. Use a test tube clamp to hold the flow meter
2. Insert the flow meter into the top corner of the central channel, facing the flow and approximately 1 meter away from the entrance of flow into the channel
3. Record the flow for 30 seconds at a sampling rate of 4 samples per second
4. Repeat steps 1-3 at all locations of the flow profile defined in Table 3, with and without the diffuser

Table 3: Flow Profile Locations

Top 1	Top 2	Top 3	Top 4	Top 5
Middle 1	Middle 2	Middle 3	Middle 4	Middle 5
Bottom 1	Bottom 2	Bottom 3	Bottom 4	Bottom 5

4.2.3 Spring Stiffness

1. Hang spring from ring stand; Place the motion sensor below the spring
2. Attach known mass to the free end of the spring
3. Zero the motion sensor at the neutral position for the spring-mass system using LoggerPro
4. Extend the spring approximately 1" and release so that the system begins to oscillate
5. Begin recording with the motion sensor; record for 20 seconds with a sampling rate of 30 samples per second
6. Find the natural frequency based on the recorded displacement data: $\omega=n/t$; where ω is the natural frequency, n is the number of oscillations, and t is the time
7. Calculate stiffness with the following formula: $k=\omega^2*m$; where k is stiffness and m is mass
8. Repeat steps 1-7 for all springs to be used in the experiments
9. Sum the stiffness of each spring used in a setup to determine the equivalent stiffness of the parallel springs

4.2.4 Cylinder Dimensions

1. Use electronic scale to measure mass of the cylinder; include end caps, and dowel pins
2. Measure the length of cylinder using a ruler
3. Measure the diameter of the cylinder using calipers
4. Repeat steps 1-3 for all cylinders to be used in the experiments

4.2.5 Natural Frequency and Damping

1. Set up the spring-cylinder system as described earlier
2. Place the system in water so that the cylinder is completely submerged
3. Use a ring stand to hold the motion sensor 0.15-0.5m above the cylinder
4. Push down on the cylinder and release so that the system begins to oscillate
5. Begin recording with the motion sensor; record for 20 seconds with a sampling rate of 30 samples per second
6. Find the damped natural frequency based on the recorded displacement data
7. Find the damping ratio based on the recorded displacement data: This derivation is discussed in the Analysis chapter
8. Repeat steps for different cylinder diameter-mass combinations; these are summarized in Table 4

Table 4: Damping Test Configurations

pvc	Diameter (m)	configuration	Mass (g)
.75"	0.0267	4 springs	135
.75"	0.0267	4 springs	152
1"	0.0334	4 springs	155
1"	0.0334	4 springs	172
1.25"	0.0422	4 springs	195
1.25"	0.0422	4 springs	212
1.5"	0.0483	4 springs	272
1.5"	0.0483	4 springs	289
2"	0.0603	2 springs	343
2"	0.0603	2 springs	377

4.2.6 Cylinder Displacement

1. Set up the spring-cylinder system as described earlier
2. Begin flow in the tank at a low speed
3. Once the cylinder begins to oscillate, record displacement and flow speed for 60 seconds with a sampling frequency of 20 samples per second
4. Increase the flow speed and repeat; flow speed was increased 5 times for each cylinder-mass configuration
5. Repeat steps 1-4 with different cylinder diameter and mass configurations; the configurations used are summarized in Table 5

Table 5: Cylinder Diameter-Mass Configurations Used in Experiments

PVC Size	Mass	# of Springs
0.75"	104g	4
0.75"	121g	4
0.75"	138g	4
0.75"	155g	4
1"	158g	4
1"	175g	4
1"	192g	4
1"	209g	4
1.25"	195g	2
1.25"	212g	2
1.25"	229g	2
1.5"	272g	4
1.5"	306g	4
1.5"	340g	4
2"	337g	2
2"	405g	2

5 Analysis and Results

This chapter presents the details of the data handling processes used in the project, as well as the final results that were produced from the collected data. Section 1 focuses on the data analysis methods used, and overviews the flow and reduction of data throughout the project. Section 2 presents a summary of the significant findings that were produced from the analysis, as well as references to the final data presented in tabular form in the appendices.

5.1 Data Analysis and Reduction Process

Throughout the experimental phase of the project, a large number of parameters were calculated based on data, theory, and a combination of both. This entire process is best summarized by Figure 25.

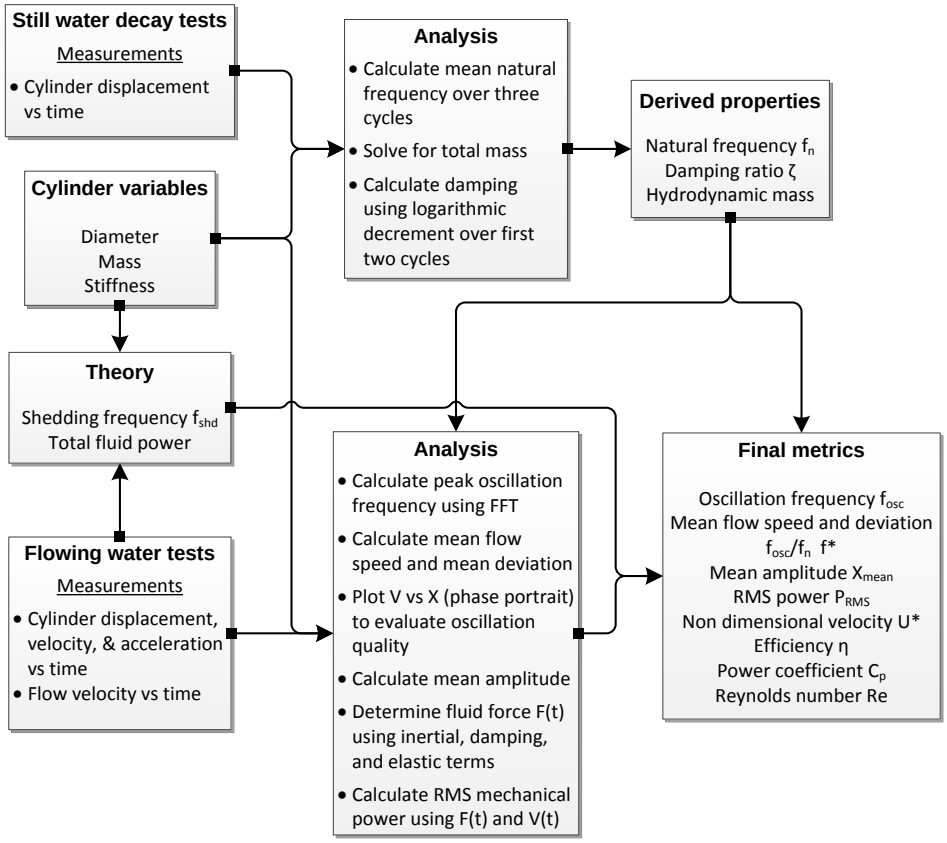

Figure 25: Experimental Data Flowchart

Here, the process is broken down into the major steps represented by each box. By viewing left to right, the process starts with the two main sets of measurements, the controlled cylinder variables, and values calculated from basic VIV and fluid theory. From here, the cylinder variables and still water tests are combined and passed through an analysis to produce the derived cylinder properties. The cylinder variables, flowing water tests, and derived properties are then passed through a second analysis, which is then combined with theory and the derived properties to produce the final metrics. The details of each of these sub-processes are described in the sections that follow.

5.1.1 Still Water Decay Tests

As introduced in the methodology, the still water decay tests consisted of measuring cylinder displacement vs. time, at 20 samples/s, after applying an initial disturbance to the cylinders in water. The data produced from these tests consisted of 5 second time series for each trial. Overall, 5 trials were performed for each cylinder configuration, which consisted of two different masses for each of the five cylinder diameters, giving a total of 50 data sets. From these data, the known cylinder diameters, masses and spring stiffness were used to determine the natural frequency (in water), damping ratio, and hydrodynamic mass of each of the five cylinders at two different values of cylinder mass. The details of these calculations are presented in the sub sections that follow. For the final summarized resultant data, see Table 6.

Table 6: Free Decay Test Summary Data

PVC	Diameter (m)	configuration	Length (m)	Mass (g)	k (N/m)	Frequency (hz)	Zeta 1	actual added mass (g)	predicted added mass (g)	ratio (actual/predicted)
.75"	0.0267	4 springs	0.22	135	47.6	1.860	0.107	214	123	1.74
.75"	0.0267	4 springs	0.22	152	47.6	1.802	0.067	219	123	1.78
1"	0.0334	4 springs	0.22	155	47.6	1.598	0.067	317	192	1.65
1"	0.0334	4 springs	0.22	172	47.6	1.587	0.067	307	192	1.59
1.25"	0.0422	2 springs	0.22	195	23.8	1.333	0.075	144	307	0.47
1.25"	0.0422	2 springs	0.22	212	23.8	1.324	0.074	132	307	0.43
1.5"	0.0483	4 springs	0.22	272	47.6	1.170	0.060	609	402	1.51
1.5"	0.0483	4 springs	0.22	289	47.6	1.138	0.052	642	402	1.60
2"	0.0603	2 springs	0.22	343	23.8	0.688	0.052	931	627	1.48
2"	0.0603	2 springs	0.22	377	23.8	0.683	0.050	916	627	1.46

5.1.1.1 Natural Frequency

The natural frequency of oscillation for each of the trials was determined using a simple averaging method. The time corresponding to the first six coherent peaks in oscillation amplitude was first recorded, where non-coherent peaks refer to the noise introduced from the initial disturbance of the cylinder. A sample trial of this process is shown in Figure 26. From there, the number of peaks (cycles) was divided by the elapsed time over the interval to yield the mean number of oscillations per unit time interval, or frequency. Combining the five total trials for each cylinder combination, the average frequency was calculated and then used as the cylinders' natural frequency in all further analysis.

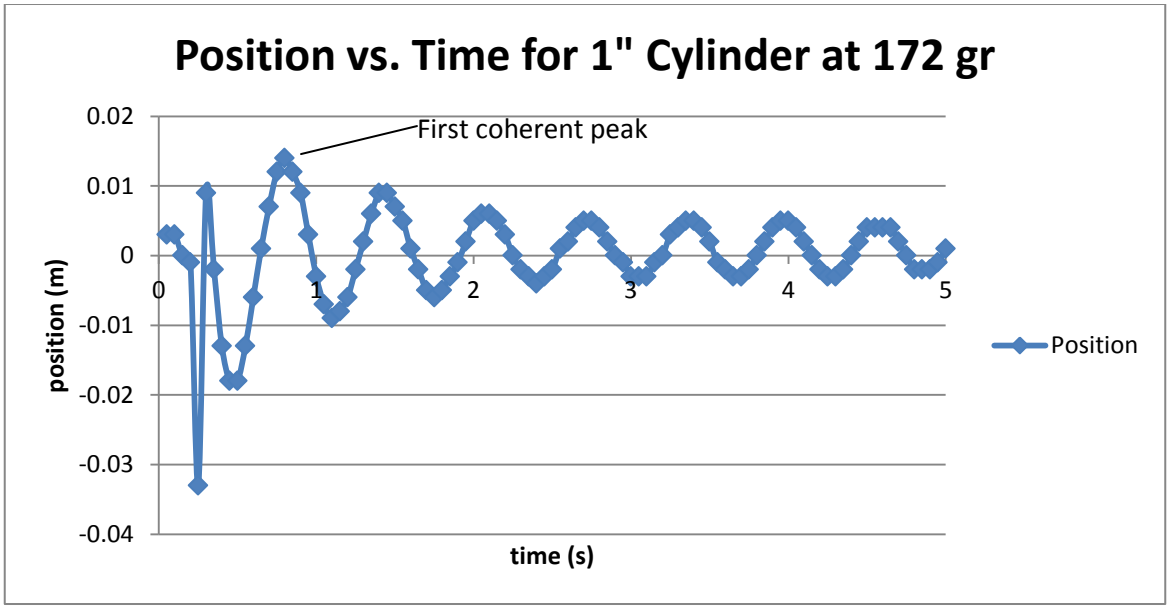

Figure 26: Free Decay Test Sample Trial

A summary of the data calculated from all the cylinders is shown in Table 10 through Table 13 of Appendix A. As can be seen, the variation of frequency between the five trials of each cylinder combination is quite small (less than 1.5% of the mean in all cases), demonstrating the consistency of cylinder natural frequency.

5.1.1.2 Damping Ratio

The damping ratio for each cylinder combination was determined using the logarithmic decrement method. The same combination of data sets as the natural frequency calculations were used. However, in this case, the amplitudes of the first three coherent peaks were recorded instead. From Figure 26, it is clear why only the first three oscillation peaks were used. It appears that after the third peak, oscillation amplitude levels out to a constant value, and ceases to decay any further during the time interval sampled. From observations made during the data collection, it is theorized that the wave-like disturbances created by the cylinder while oscillating were reflected throughout the test tank. Upon returning to the cylinder, these waves likely sustained the cylinder oscillations when they would normally continue to decay in amplitude.

The values of the first three oscillation peaks were first used to define a new value δ, where $\delta = \ln(\frac{A_i}{A_{i+1}})$, and A_i represents the amplitude of the i^{th} peak. Since three values of A_i were used, two corresponding δ's were calculated. From here, the damping ratio ζ was calculated from Eq. 5-1.

$$\zeta = \frac{\delta}{\sqrt{(2\pi)^2 + \delta^2}} \qquad \textbf{Eq. 5-1}$$

This method produced two values of the damping ratio for each trial, as can again be seen for all cylinders in Appendix A. Unlike the natural frequency data, the values of ζ for each trial showed significant variation both between one another and between trials. Again, the mean value of the damping ratio was determined from the five values calculated for each cylinder combination. In light of the wave-like disturbances mentioned previously, it was decided that only the first of the two sets of ζ's from each trial would be used, since they were less likely to be influenced by the disturbances. In the calculations that followed, it was these mean values of $\zeta 1$ which were used for each cylinder combination.

5.1.1.3 Hydrodynamic Mass

As introduced in the modeling chapter, hydrodynamic mass refers to the additional mass which is effectively added to the cylinder by the fluid it displaces. The theory for cylindrical bodies states that this mass is equal to the mass of the fluid occupied by a volume equal to that of the cylinder. To determine this value for the different cylinder combinations, the previously calculated natural frequencies were used in combination with the known cylinder masses and spring stiffness.

Basic vibration theory gives the damped natural frequency of a body as Eq. 5-2,

$$f_n = \frac{1}{2\pi}\sqrt{\frac{k}{m}} * \sqrt{1-\zeta^2} \qquad \textbf{Eq. 5-2}$$

where k is the total stiffness and m is the total mass. By solving for the total mass and then subtracting the known cylinder mass, the hydrodynamic added mass was effectively determined. Since this value was determined using mean natural frequencies, only one value is calculated for each cylinder-mass combination, and the results are again shown in Table 6. As can be seen there, there was a significant discrepancy between the hydrodynamic mass specified by theory, and that calculated experimentally. A possible explanation of this can be given based on the separation distance of the cylinder from the bottom surface of the channel during the trials. Since this distance was relatively small, on the order of <5 cylinder diameters, additional “added inertia” could be imparted to the cylinder since the assumption of infinite fluid, from which added mass theory is based, is not valid. Despite these findings, the flowing water tests which were to be later conducted would have the same physical setup, so use of the experimentally determined hydrodynamic masses was an appropriate choice.

5.1.2 Flowing Water Tests

As introduced in the methodology, the flowing water tests consisted of 85 total cylinder trials. For each of the five cylinder diameters, two to four different cylinder masses were used, and each of those combinations was subjected to four to five unique flow speeds. The specific testing combinations used were previously listed in the methodology. The data set produced from each individual trial consisted of a one minute time series of cylinder displacement and flow velocity. The data logging software also numerically differentiated the displacement data and included cylinder velocity and acceleration in the data set as well. These data were then analyzed in combination with the controlled cylinder variables and derived properties found in section 5.1.1 in order to determine mean flow speed, oscillation frequency, f*, mean oscillation amplitude, RMS mechanical power, U*, efficiency, power coefficient, and Re for each cylinder test trial. The details of these calculations are presented in the sub sections that follow. For reference, a sample of this final data is presented in Table 7 below. The complete results for all valid tests are then shown in Appendix B.

mean flow (m/s)	SD %	F_{shd} (hz)	F_{osc} (hz)	osc/shd	f*	X mean (m)	Prms (W)	U*	η	Cp	Re	A/D
0.250	7.0	1.85	1.92	1.04	0.98	0.013	0.0169	4.79	0.37	0.37	5.09E+03	0.49
0.246	6.8	1.82	1.98	1.09	1.01	0.016	0.0213	4.72	0.49	0.49	5.01E+03	0.60
0.251	6.6	1.86	1.96	1.05	1.01	0.016	0.0213	4.82	0.46	0.46	5.12E+03	0.60
0.273	9.7	2.02	2.10	1.04	1.07	0.018	0.0272	5.24	0.46	0.46	5.56E+03	0.67
0.301	5.8	2.23	2.12	0.95	1.09	0.018	0.0302	5.78	0.38	0.38	6.14E+03	0.67
mean	**7.2**								**0.43**	**0.43**		**0.61**

Table 7: 0.75" Cylinder Trial 1Final Results

The data shown in Table 7 depicts the results from one specific mass trial of the 0.75" cylinder. All of the metrics mentioned above are shown, as well as a few additional derived ratios which provide a useful reference. Mean flow speed is simply the time averaged flow velocity measured over the one minute test interval. SD% gives the standard deviation of the flow speed time series as a percentage of the mean value. F_{shd} represents the theoretically calculated vortex shedding frequency for the given mean flow speed and cylinder diameter. f_{osc} gives the experimentally determined peak frequency of cylinder oscillation. osc/shd simply gives the ratio of f_{osc} to f_{shd} for the purpose of determining how closely the two matched. The non-dimensional f* is the ratio of f_{osc} to f_n, again for comparing the behavior of the observed frequencies. X mean represents the mean cylinder oscillation amplitude over each time series. P_{rms} gives the root mean square value of the experimentally calculated mechanical power of the cylinder. U* is the non-dimensional velocity parameter introduced previously. η gives the power harnessing efficiency, comparing P_{rms} to the theoretical fluid power over the cylinder cross-sectional area. C_p is the power coefficient, given by $P_{rms}/.5\rho DLU^3$, which also represents efficiency. Re is the Reynolds number for the flow conditions based on the cylinder diameter as a characteristic length. Finally, A/D gives the ratio of mean oscillation amplitude to cylinder diameter.

In the sections that follow, the details of calculating some of the parameters discussed above are presented. A majority of this analysis was performed using a custom MATLAB script that automatically imported the desired experimental data file and then prompted the user to enter several previously known values; specifically, the sampling rate, total cylinder mass, spring stiffness, and damping ratio. With the exception of a Fast Fourier Transform algorithm, the script did not perform any particularly complex calculations that couldn't otherwise be accomplished in spreadsheet software. The choice of using a script to analyze each data file was made mostly for convenience, since it automated the process. In light of this, the code within the script will only be referenced in the case of the FFT, where multiple decisions are required in implementing the calculation. In all other cases, only simple arithmetic was being performed, and a description will be given in general terms without reference to the script.

5.1.2.1 Flow Speed

Due of the limitations of the experimental setup, the ability to maintain a constant flow speed for each cylinder trial was poor. Because of this, it was only possible to characterize each trial by a mean flow speed. A well representative example of a time series for flow speed is shown in Figure 27. The solid red line gives the mean value, while the shaded red band denotes a range of one standard deviation from the mean. Considering the relatively small range of flow speeds which were achievable, such variation for an individual trial was an obvious shortcoming of the physical setup. Despite this, it was generally found that unique mean flow speeds did produce unique values of the other measurements, even though the flow speed ranges of different trials overlapped.

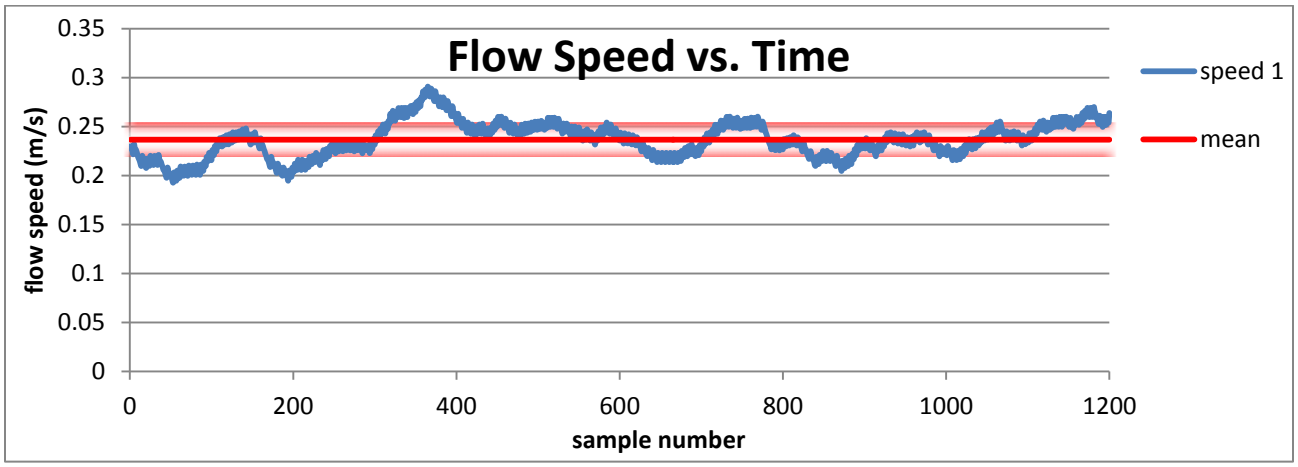

Figure 27: Flow Speed Time Series from 1" Cylinder

5.1.2.2 Oscillation Frequency

To determine the cylinder oscillation frequencies from each of the displacement time series, a discrete fast Fourier method was used. This is in contrast to the averaging method used to determine natural frequencies in the still water tests. To accomplish this, the built in discrete fast Fourier transform (FFT) function in MATLAB was used. From here, the peak frequency was evaluated by determining the frequency corresponding to the largest FFT amplitude. Because of the very well defined single amplitude peaks, it was decided that it was appropriate to characterize each cylinder trial by this peak frequency. The code used to accomplish this is shown below in Figure 28, and the details are discussed in what follows.

```
importfile(input_file);

w = x0x22Acceleration0x22;
v = x0x22Velocity0x22;
y = x0x22Position0x22;
x = x0x22Time0x22;
z = x0x22FlowRate0x22;

T = 1/Fs;                       % Sample time
L = length(y);                       % Length of signal
t = (0:L-1)*T;                  % Time vector

NFFT = 2^nextpow2(L); % Next power of 2 from length of y
Y = fft(y,NFFT)/L;
f = Fs/2*linspace(0,1,NFFT/2+1);

% Plot single-sided amplitude spectrum.
figure('visible','on');
plot(f,2*abs(Y(1:NFFT/2+1)));
title(strcat(input_file,' - Single-Sided Amplitude Spectrum of y(t)'))
xlabel('Frequency (Hz)')
ylabel('|Y(f)|')

temp = 2*abs(Y(1:NFFT/2+1));

[max_val, peak_freq] = max(temp(51:end));
peak_freq = peak_freq + 50 ; % Adjust for removing first 50 values from temp
peak_freq = f(peak_freq);
```

Figure 28: MATLAB FFT Script

The script is run for each individual data file generated from the experimental trials. The variables v through z are then defined as vectors from the individual columns of the data file. The period T is defined based on the user-input sampling rate (20 hz for most trials). A new time vector t is then defined based on T and the sample length of the data file. The algorithm requires that the signal have a number of data points equal to 2^N, where N is an integer, so the signal is padded with zero values to make it the appropriate length. A frequency vector f is then defined based on half the sampling rate (Nyquist frequency), and the modified signal length. From here, the single sided amplitude spectrum was plotted for evaluation, as seen in Figure 29. To determine peak frequency, the maximum value of the single sided amplitude is found and the associated frequency returned. The previously added zero values cause a large amplitude spectrum peak at a frequency near zero, so the determination of peak amplitude is made starting from the 51^{st} data point. This method effectively removes the influence of the padded zero data.

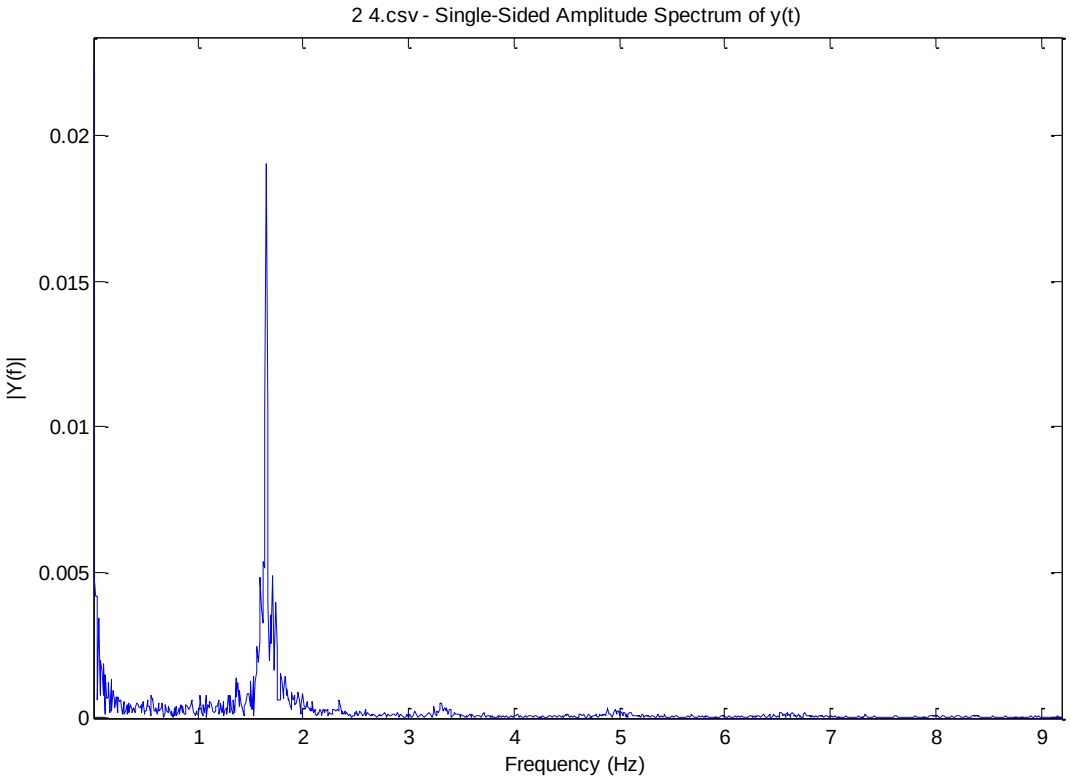

Figure 29: 1.0" Cylinder Single Sided Amplitude Spectrum

5.1.2.3 Mean Amplitude

The mean cylinder oscillation amplitude over each time series was determined by generating a phase portrait, or plot of velocity vs. position, for each data set. This method was found to be far superior to individually determining each amplitude peak. A phase portrait representative of most of the experimental data is shown by the blue trajectory in Figure 30.

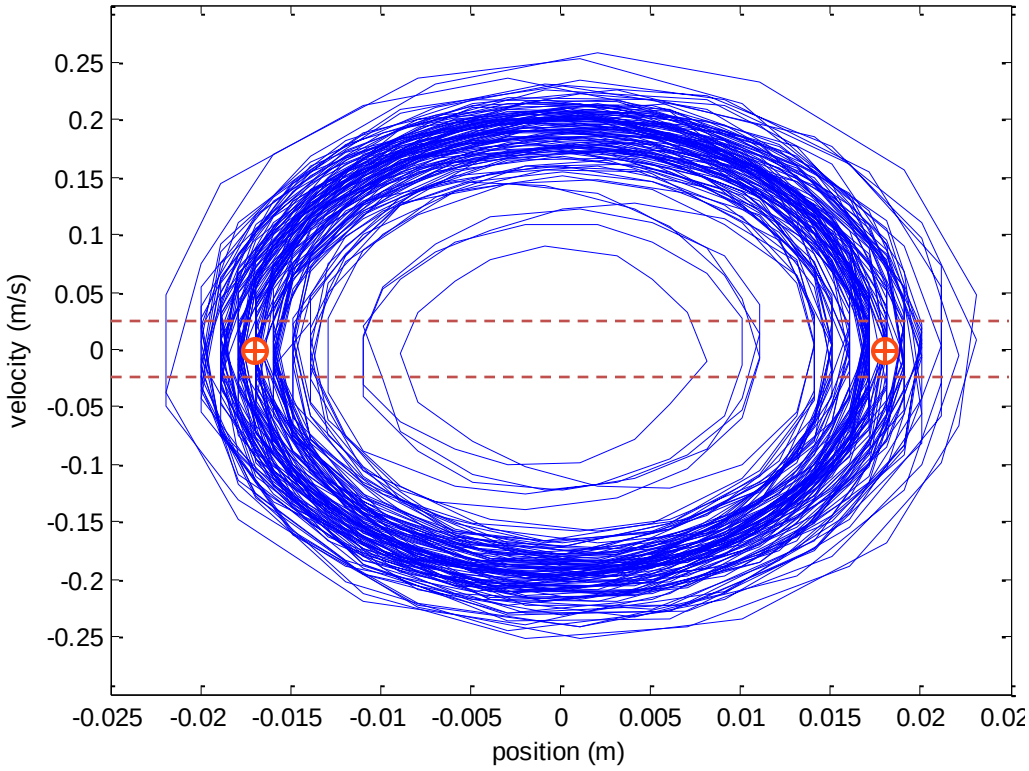

Figure 30: 0.75" Cylinder Phase Portrait

The concentric rings can be thought of as being the path traced out as time elapses. As can be seen, the locations near zero velocity correspond to peaks in the position value. This is intuitive, since the cylinder should reach zero velocity at the peak of its oscillation. The dashed red lines represent a region containing the lowest 10% of velocity values. The mean peak amplitude is then found by evaluating the mean absolute value of the position data within this region. The result is an amplitude reflective of the locations shown by the red circles.

5.1.2.4 Potential Mechanical Power

The potential mechanical power transferred to the cylinders from the fluid was experimentally determined using the same relations demonstrated in the modeling chapter. The differential equation relating fluid force to cylinder behavior is given by Eq. 5-3.

$$my'' + 2m\zeta\omega_n y' + ky = F(t) \qquad \textbf{Eq. 5-3}$$

In this case, information for all the parameters and variables on the left side of the equation is known from the experimental measurements and data. Using the experimental values along with the cylinder oscillation data allowed the fluid force F(t) do be determined over each trial. From there, F(t) was multiplied with the cylinder velocity data to produce a time series of mechanical power P(t). Finally, the root mean square value of P(t), P_{RMS}, was calculated to produce a single metric for each cylinder trial, as given by Eq. 5-4.

$$P_{RMS} = \sqrt{\frac{\sum_i^L P_i(t)}{L}} \qquad \textbf{Eq. 5-4}$$

The parameter L is simply the length of the P(t) vector. Inherently, this representation of power is slightly misleading, since it refers only to the power being transferred to the cylinder. Actual extractable power, in the form of electricity generation, would necessarily be reduced by the losses in the extraction process. Despite this, the power determined here provides a useful baseline of the maximum potential power that could be extracted.

5.2 Results & Discussion

The final phase of this project consisted of interpretation and comparison of the numerical results produced from the analysis described in section 5.1. The final data were further reduced by attempting to collapse specific metrics from all cylinder trials onto single plots, making use of the various non-dimensional parameters that were previously determined. This section presents the final data plots that were determined to show meaningful or significant trends. Additionally, this section provides an overall discussion of the observations and findings made throughout the entire project, both quantitative and qualitative. As a note, the data generated from the 1.25" cylinder was found to be unusable due to the fact that the cylinder was reaching the shut height of the springs, seriously affecting the oscillations.

5.2.1 Oscillation frequency

All of the tests were performed at U* values between four and eight. According to lock-in theory, the range of U* for which lock-in is most likely to occur is centered on a U* of five. Although this was known a priori, it was not actively used in the experimental design process, where the focus was on attempting to match cylinder natural frequency to predicted shedding frequencies. However, significantly different experimental values of cylinder mass, hydrodynamic mass, and flow speed were found compared to the values used in the initial model.

One of the initial hopes of testing was to experimentally find the boundaries where VIV ceases. In reality, limitations of the experimental set up resulted in test measurements entirely within the ideal lock-in range. Due to this, it was not possible to determine the cutoff values of U* for which no significant cylinder oscillation occurs. Despite this, the final comparison of frequency to U* shown in Figure 31 has several interesting features.

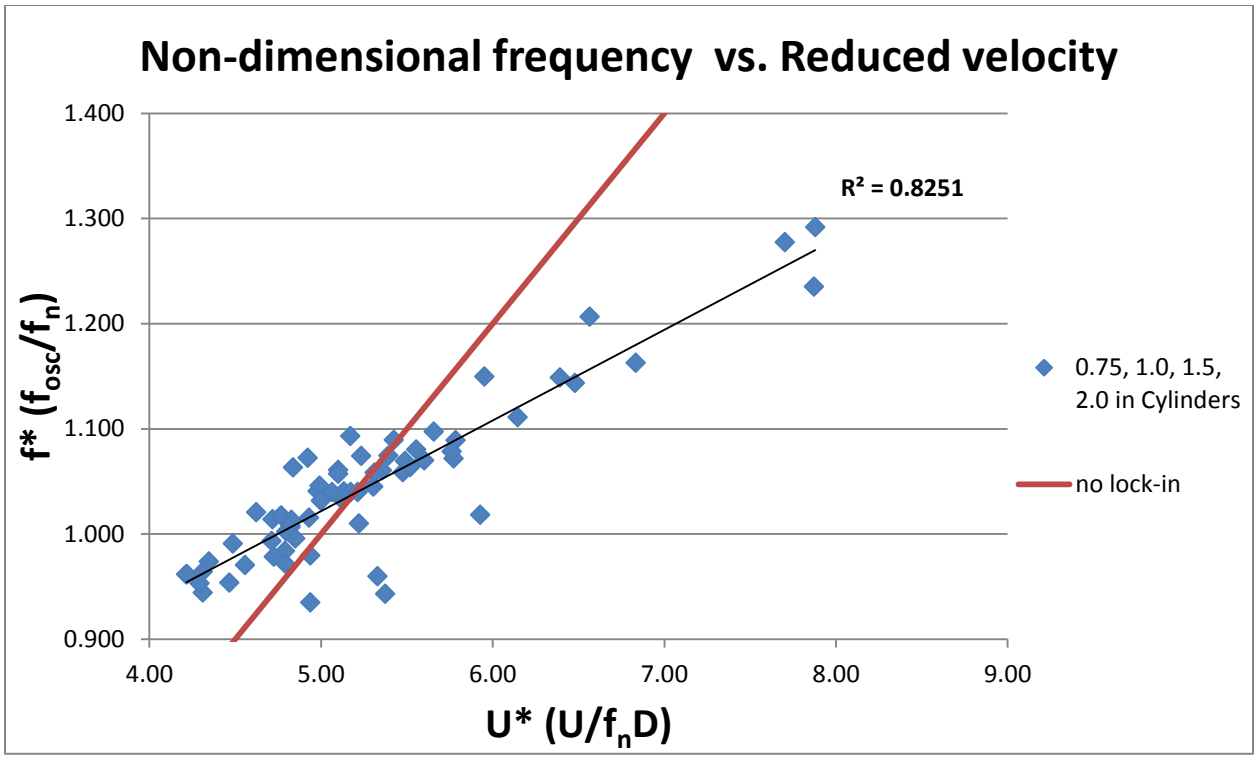

Figure 31: Non-Dimensional Frequency Results

The data presented in Figure 31 shows a total of 65 cylinder trials; nearly all of the tests from the 0.75, 1.0, 1.5, and 2.0 inch cylinders. The thin black line represents a best fit linear trend, with a correlation coefficient of 0.825. As can be seen, with the exception of several outliers, the data shows very close grouping particularly around the lower range of U*. The linear nature of the data trend agrees with theory on the basis that vortex shedding frequency, and accordingly, oscillation frequency, increases linearly with flow velocity for a given cylinder diameter, which is identical to increasing linearly with U*. The red line represents a theoretical f* trend in which the shedding frequency does not shift to match the cylinder natural frequency, but simply increases linearly according to the Strouhal relation. The slope of this line has the constant value of S=0.2. Using this no lock-in relation, f* attains the value of 1 at a U* value of 5. The trend line for the experimental data has a smaller slope, but still intersects f*=1 near a U* value of 5. This change in slope demonstrates a partial frequency shift from the shedding frequency to the actual observed oscillation frequency. Full lock in would present itself as the oscillation frequency precisely matching the cylinder natural frequency, resulting in an f* value of 1 independent of U*, which would appear as a horizontal line on the plot. The

change in slope observed with respect to the no lock-in line towards a horizontal line signifies that some frequency shift did occur. The margin of error throughout all the experimental measurements could partially account for the discrepancies between full lock-in and the experimental data, but overall the lack of complete lock-in is an inconclusive result. For this reason, we recommend higher levels of precision and adjustability of the test set up for any future work, as well as more realistic testing conditions.

5.2.2 Power Coefficient

A non-dimensionalized power coefficient was calculated for each of the valid experiments. These were then plotted against the respective Reynolds Numbers, as shown in Figure 32. The plot show that the power coefficient decays logarithmically with Reynolds Number towards an asymptote at a power coefficient of 0.1. Ideally, the potential mechanical power could be predicted based on this relationship, but given the disagreement between theory and experimental data, it is unknown if this curve could be used to extrapolate for values of Re far outside of this range.

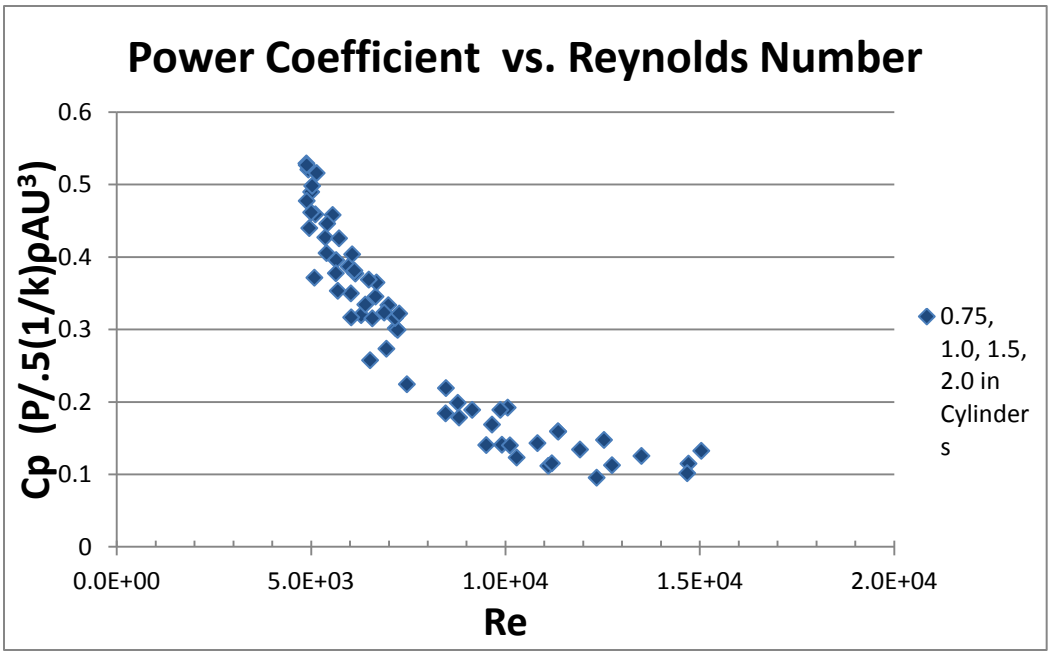

Figure 32: Plot of Power Coefficients vs. Reynolds Number

5.2.3 Power Harnessing Efficiency

The efficiency of the energy transfer from the fluid acting on the cylinders was plotted against the respective reduced velocity U*, as shown in Figure 33. The peak efficiency was over 50% for the 0.75" cylinder. The efficiencies were lower for the larger cylinders and higher velocities. The relationship between cylinder size and efficiency appears stronger than the relationship between efficiency and velocity. The minimum efficiency was down to 10% for the 2 in cylinder at the maximum reduced velocity achieved. The length for all the cylinders was constant. The relationship between the diameter of the cylinder to the length, or the aspect ratio is 1:8.6 for the 0.75in cylinder. The aspect ratio is 1:3.8 for the 2in cylinder. These results show that the efficiency is higher for slender cylinders. The VIVACE experiments had determined that the ideal value for the aspect ratio is 1:8. Future experiments should test both high and low aspect ratio cylinders to further develop an understanding between aspect ratio and efficiency.

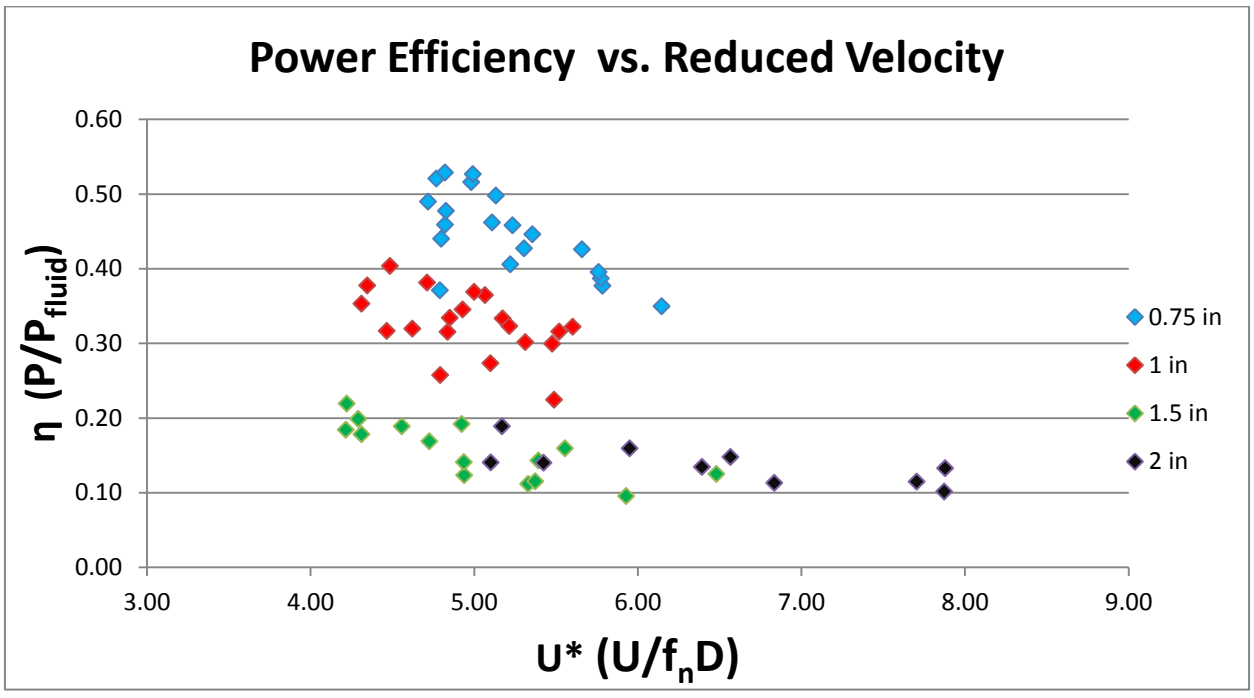

Figure 33: Power Efficiency vs. Reduced Velocity

5.2.4 Damping

Damping in the experimental system was due almost entirely to the fluid and ranged from a damping ratio of about 0.06 to 0.1. The damping would necessarily be much larger in a system with a power take off mechanism. Figure 34 is an example of the potential mechanical power plotted for each of the contributions from the inertial, damping, and elastic terms of the differential equation for fluid force. The contribution from damping is small in comparison to the contributions of the other two terms. If damping were to be increased significantly, it would have a larger impact on the net power. On this small scale, significant amounts of additional damping would have likely halted the oscillations. Accordingly, further tests should be conducted at higher velocities so that more fluid force is available to overcome greater values of damping. These experiments could then be used to optimize the extractable power while still maintaining cylinder oscillations.

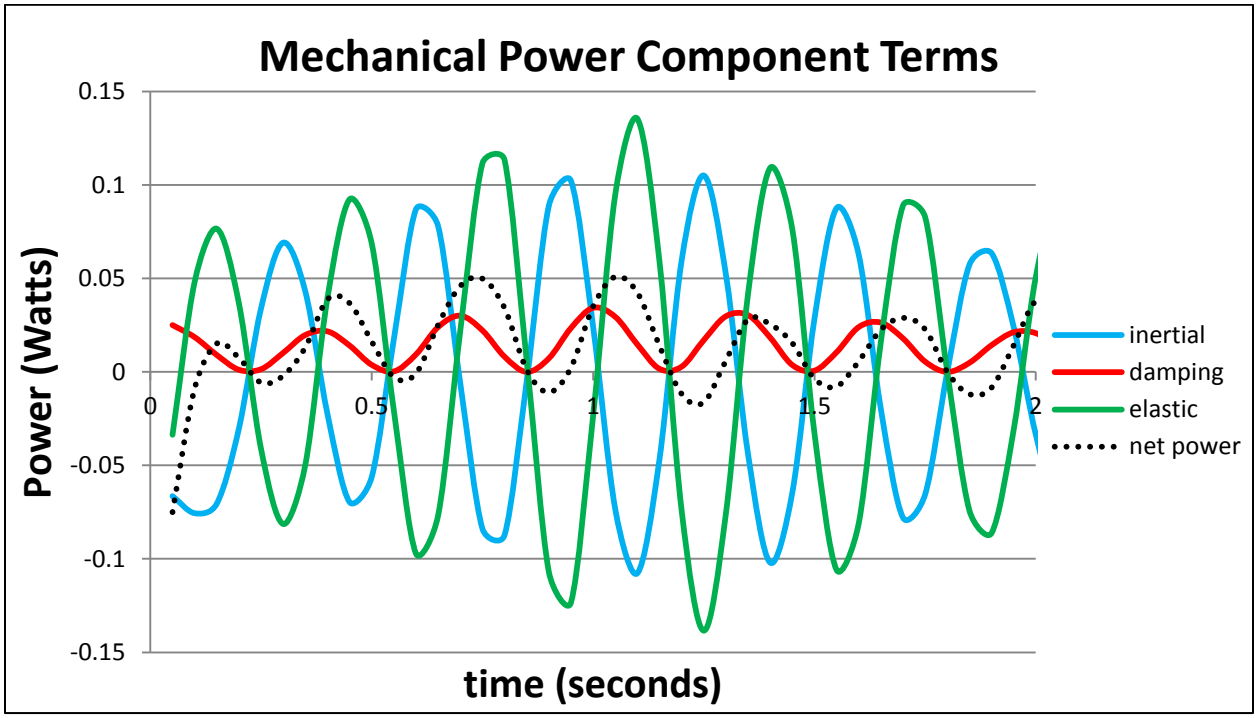

Figure 34: Mechanical Power Component Terms

5.2.5 Hydrodynamic Mass

As discussed previously, the experimentally determined value for the added mass of a cylinder was about 1.5 times greater on average than the theoretical values. The added mass should be equal to the mass of the fluid volume displaced by the cylinder. The testing conditions may have contributed to this difference. The small gap between the cylinder and the surroundings of the cross-section may have increased the inertia needed to displace the volume of the fluid. Future experiments should have a larger gap between the cylinder and the boundaries to limit the effects on added mass. Since most calculations were based on the experimentally determined added mass, the same experiments conducted under different test setups would have different end results. Ensuring that the experimental added mass closely matches the theoretical added mass for all future experiments would allow for more accurate comparisons between experiments.

5.2.6 Power Density

Assuming set distances between cylinders in a power plant array, power density, modeled in Figure 35 below, the power density of the array can be calculated as a function of cylinder diameter. Distances t and p shown below are linear functions of diameter.

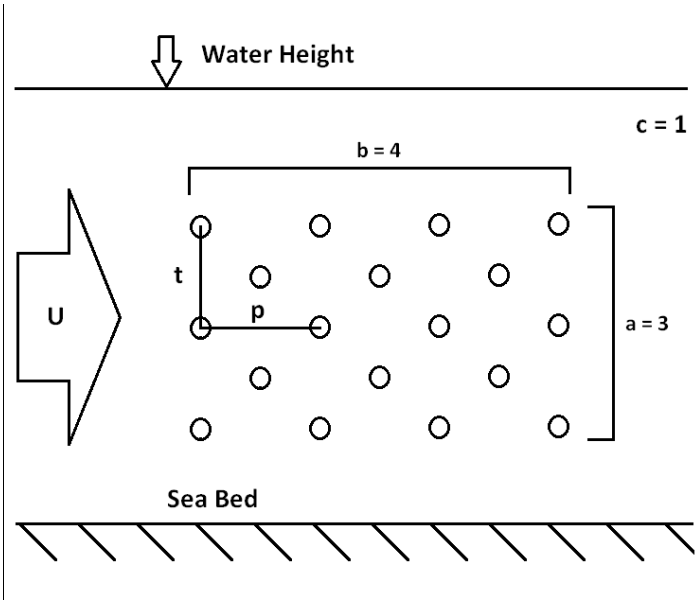

Figure 35: Power Density Schematic

VIVACE proposes the staggered cylinder arrangement from Figure 35 based on relationships of t and p shown in Eq. 5-5 and Eq. 5-6 below.

$$p(D) = 8 * D \quad \textbf{Eq. 5-5}$$

$$t(D) = 5 * D \quad \textbf{Eq. 5-6}$$

The number of cylinders and resulting volume (*V(D)*)of the array can be calculated using Eq. 5-7 and Eq. 5-8 below, where *a* is the number of cylinders deep in flow direction, *b* is the number of cylinders tall, and *c* is the number of *a* x *b* arrays into the page.

$$N_{cylinders} = a * b * c + (a-1)(b-1) * c \quad \textbf{Eq. 5-7}$$

$$V(D) = [a * t(D)] * [b * p(D)] * (c * L) \quad \textbf{Eq. 5-8}$$

The maximum total available power in the model is the number of cylinders times the maximum calculated RMS power for that cylinder diameter (Eq. 5-9). The maximum power density (Eq. 5-10) is a function of cylinder diameter is given by the maximum total power over the array volume.

$$P_{total} = N_{cylinders} * P_{rms} \quad \textbf{Eq. 5-9}$$

$$PD(D) = P_{total}/V(D) \quad \textbf{Eq. 5-10}$$

Table 8: Power Density by Cylinder Diameter

Nominal Dia. (in)	Diameter (in)	Max Power (RMS) (W)	PD (W/m^3)
0.75	1.050	0.0302	9.1
1.00	1.315	0.0606	10.3
1.25	1.660	0.0459	5
1.50	1.900	0.0326	2.5
2.00	2.375	0.0613	2.6

Table 8 shows the maximum RMS power calculated from experimental data by nominal cylinder diameter, and the resulting calculated power density for a single cylinder array.

This model can be used to establish a reasonable estimate of power density for the proposed future cylinder. Assuming 50% efficiency for both water to cylinder power conversion and cylinder to electrical conversion, Eq. 5-11 may be used to solve for cylinder power.

$$P = 0.25 * \rho * L * D * U^3 \quad \textbf{Eq. 5-11}$$

For one test using the 0.75” cylinder, with 0.24 m/s measured flow speed, this was found to be accurate. Extrapolating this relationship to the larger proposed parameters yields the relationship shown in Eq. 5-12.

$$P = 0.25 * \rho * 4\,''* 36" * (1\ m/s)^3 = 23\ Watts \quad \textbf{Eq. 5-12}$$

Resolving Eq. 5-9 and Eq. 5-10 using D = 4in and P_{RMS} = 23W yields an estimated power density of 60 W/m^3 for a single cylinder. Increasing array size by increasing the value of *a* and *b* yields an upper limit of power density at about 120 W/m^3.

5.2.7 Cylinder Amplitude

It was found that cylinder amplitude generally increased with an increase in flow speed. According to existing theory, amplitudes in the range of 1-2 diameters are reasonable; however our experiments never resulted in amplitude above 1 diameter. This result is likely influenced by the scale of the experimental set up. First, flow velocities used in this experiment are in the lower range of VIV inducing speeds. Increasing the flow velocity to a velocity range of 1-3 m/s as recommended for future testing may yield higher amplitude vibration. Also, amplitude may have been limited by the small range of available space for the cylinder to vibrate. The extension springs used in this experiment were seen on a few occasions to reach shut length. Linear stiffness range for springs should generally be assumed to be from 15-85% of spring extension. Stiffness varies nonlinearly outside this range, and for this small scale experiment, the change in stiffness may have affected the overall amplitude.

A limitation of the mathematical model is that the estimate for cylinder vibration amplitude did not take the self-limiting effect into account. This seemed a reasonable assumption during the mathematical modeling stages of the project, but came into question after compiling the test data. As a result, experimental findings range both above and below the model predictions for maximum cylinder amplitude.

To compensate for these deviations in experimental results from VIV theory, the future testing set up design has been based on the theoretical maximum amplitude over diameter ratio (2.5-3). It is expected that in a more robust future test model, testing data will more closely agree with theory.

5.2.8 Observations

It was observed while testing that placing one's hand 2 or 3 inches in front of the cylinder did not significantly inhibit vibration of the cylinder. It was also estimated that the force of the cylinder pushing up on one's hand while an object was 2 or 3 inches in front of the cylinder remained about the same. This leads us to believe that aquatic obstructions, either wildlife or debris that enter the path of water over the cylinder, will not have a significant effect on the vibration.

It was also seen through comparison of flow velocity to cylinder position, velocity, and acceleration data that measured spikes in the flow velocity did not result in quantifiable changes in the cylinder oscillation frequency. There are a few possible reasons for this. First, resolution of the flow rate sensor was 1.2 mm/s. Also, a limitation of measuring with the flow rate sensor and displacement sensor simultaneously was that a uniform sampling frequency needed to be specified. The recommended sampling frequency for the flow sensor was 4 Hz, up to 50 Hz for the displacement sensor, while 20 or 30 Hz was used during the experiment.

6 Recommendations for Future Work

This section outlines potential future work to be done in a continuation of this project. Design of future test set up is discussed as well as experiments to be conducted.

6.1 Project Continuation Proposal

The previously discussed experiments were conducted at flow speeds up to approximately 0.35m/s. These speeds are significantly lower than those found in ocean currents and river flows. Increasing the Reynolds number by increasing fluid velocity by an order of magnitude to 1-3 m/s, and increasing cylinder diameter by a few inches would allow for results that could more accurately predict the potential for the technology under realistic conditions. Because of the low velocity for the fluid in the initial experiment, the lift force of the fluid acting on the cylinders was also small. This lift force could only overcome small amounts of damping and so damping was limited to the damping caused by the fluid. The vibrations of the cylinders subjected to fluid flow can only perform useful work if a system exists to extract the energy. Any power take off system would significantly increase the damping of the setup. The lift force of the fluid acting on the cylinder is dependent on the velocity of the fluid squared. Thus increasing the fluid velocity by an order of magnitude would increase the lift force by a factor of 100. This larger lift force would be able to overcome the damping introduced by a power take off mechanism and would allow for experiments that can truly test the potential for power generation.

It is proposed that future participants in this project area assess the possibility of use of large scale test facilities such as those at the Alden Research Laboratory. The Alden Research Laboratory in Holden, MA is the oldest continuously run hydro research facility in the United States. The company prides itself on using its resources to support the future of clean, renewable hydro energy. Numerous test flumes and tanks exist at the site for the testing and optimization of hydrokinetic equipment. Many of these facilities are capable of testing prototype turbines at full scale operating velocities. The company's newest flume has a test section of 80x20x10 feet with a flow rate of 500 cubic feet per second. With guide walls, the

flow can be channeled to produce velocities up to 10ft/s or 3m/s. The flume functions similarly to the flow tank developed for the discussed experiments, but on a much larger scale. The flume is a closed loop, two-level system that incorporates twin axial flow pumps to generate a flow through the test section. A schematic of the flume is shown in Figure 36.

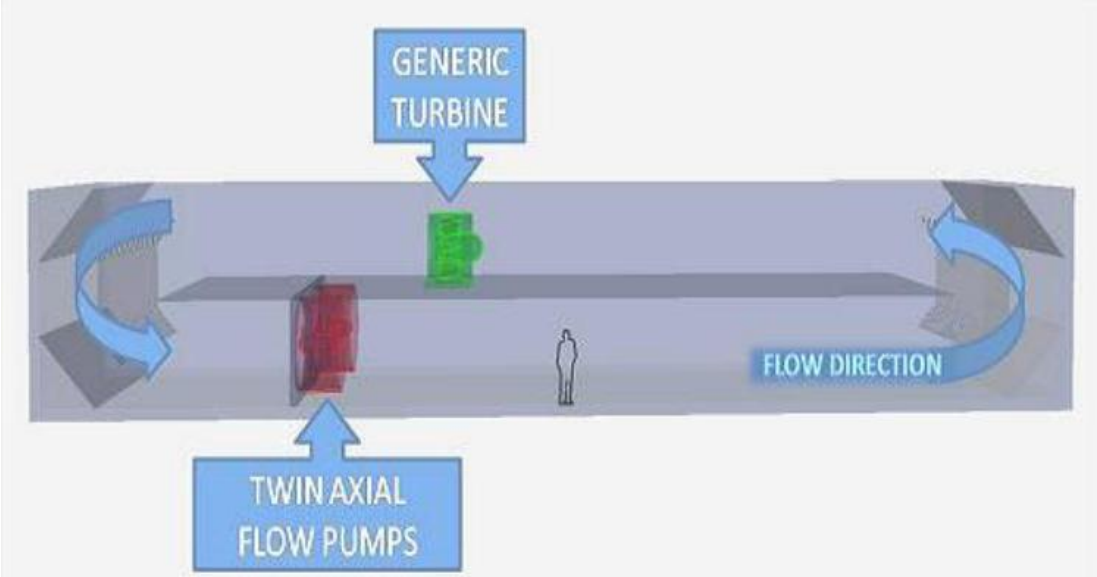

Figure 36: Schematic of the Alden Labs Test Flume

These facilities provide greater flow speeds with greater control than the testing setup used in the discussed experiments. The use of such testing conditions would increase the flexibility of future experiments and lead to a better understanding of the potential for vortex induced vibrations as a source for clean energy.

6.2 Task Specifications

Under the new proposed testing conditions, a new test rig will need to be designed. Below is an initial list of some of the recommended task specifications.

1. **Device must accommodate the installation and data measurement of interchangeable cylinders, or other geometry, 1 meter in length.**

An important component of future testing in this area is the addition or simulation of a power take off system. Both methods introduce a larger amount of damping into the total force acting on the cylinder. One way to increase the amount of damping the system can

handle without stopping oscillation is to increase the cylinder mass. A larger cylinder will be able to withstand a greater amount of damping which will allow realistic power take off and efficiency calculations. Interchangeable cylinders will make the testing process easier.

With this larger scale, linear bearings will be necessary to constrain the cylinder to motion in the transverse direction. Since the bearings will be secured to their respective tracks, it follows that the interface between cylinder and bearing will be the joint around which interchangeability is necessary. The bearing will be contained within a part (slider) that contacts the cylinder. Assuming the cylinders are hollow with end caps, one way to ensure interchangeability is to drill holes of a set size into the cylinder end caps and design the slider to hold the cylinders using these holes. Bearings can be located either in or out of the water. The Igus Company manufactures low cost plastic linear bearings for underwater applications.

2. **Device must accommodate cylinders of varying aspect ratio from 1:10 to 1:6.**

Cylinders or shapes of other geometry of varying aspect ratio must be used to more easily explore optimal aspect ratio ranges. Other types of geometry with a uniform cross section may be considered as well.

3. **Device must allow for a 3*diameter amplitude test area during flow testing.**

An assumption from experiments conducted in this project, and reinforced by further research, is that oscillations of amplitude greater than 3 times the cylinder diameter are not expected. The test set up in this project did not allow the larger cylinders a full range of oscillation in some cases because the channel was not tall enough. Therefore, this specification will allow for a maximum range of oscillation of 1m for the cylinder with aspect ratio of 1:6.

4. **The height of the test area and cylinder must be adjustable to a range of 3ft, unless constructed for testing for a flow channel of known water height and gap value calculations are conducted to establish an acceptable test area height.**

A disadvantage of the tests conducted in this project was that in some cases, the distance between cylinder and channel bottom or cylinder and water height was less than required according to gap value calculations. This likely contributed to the variation in

apparent mass calculations. To accurately analyze a cylinder of given mass, these calculations should be accounted for.

5. **In addition to the mass of the cylinders, the mass of the testing rig will not exceed 10kg.**

The force of lift would be significantly greater at the high velocities. Nevertheless, if the mass of the test rig is too great, the force will not be strong enough to force the setup to oscillate. This mass includes end caps for the cylinders, sensors, springs, and the frame used to hold the cylinder. It does not include the hydrodynamic mass of the cylinder or the mass of the cylinder itself. Thus, this value should be constant for all experiments independent of the cylinder size. The maximum force of lift for these cylinder sizes and flow speeds in the lock-in range will be approximately 40-130N.

6. **The stiffness of all springs storing cylinder energy must be adjustable.**

As a result the limit of cylinder size and flow speed in the test set up in this project, only a small range of spring stiffness was available to provide lock-in, and stiffness was not adjustable. Adjustable spring stiffness in this device will enable easier testing at a wider range of mass and other parameters. The range for the total stiffness of the system is 4000N/m to 7000N/m. The formula

$$k = \frac{G * d^4}{8 * D^3 * N}$$

where k is stiffness, G is the shear modulus, d is the wire diameter, D is the outer diameter and N is the number of active coils, provides an approximation for the stiffness of a spring. Reducing the number of active coils will increase the stiffness of the spring. This will allow for the same spring to provide multiple values of stiffness. A compression spring could be screwed onto a threaded bolt with the correct pitch and diameter to reduce the number of active coils and increase the stiffness. To achieve the listed specification, each spring will need a stiffness of 2000N/m. The shear modulus for steel is approximately 80 Gpa. A spring with a diameter of 0.01m and wire diameter of 0.0012m will have 13 coils. From the McMaster-Carr Catalog, a spring with these specifications is available with a length of 0.076m. Reducing the active

number of coils to 7 would achieve the max stiffness of 3500N/m I each spring. Many spring manufacturers will create custom springs based on requirements for length, pitch, stiffness, and diameter. A longer spring would be needed to accommodate the amplitude of oscillations.

7. **The damping of all dampers affecting cylinder motion during testing must be adjustable.**

Adjustable damping is critical to the available power optimization testing. Damping must be optimized with cylinder oscillation and must be high to simulate power extraction but not so high as to critically interfere with the vibrations. In future testing, this relationship must be tested and established.

8. **The device must be compatible with one or more high resolution or analog linear displacement sensors.**

A disadvantage of tests conducted in this project was sensor resolution. To avoid resolution issues, an analog sensor such as a linear variable differential transformer (LVDT) could be used, which converts linear motion to a signal using the motion of a magnet over a coil.

Stellar Technology Inc. offers the LLC65X, a 37 inch stroke linear displacement LVDT, which matches the absolute maximum displacement range required according to Task Specification 3. Different LVDTs are available for either out of water or underwater use.

9. **The cylinders will be Schedule 10 aluminum pipes.**

PVC pipes for the proposed sizes for the cylinders are too light to achieve the proper natural frequencies for lock-in. Aluminum pipes will provide a suitable mass that is not too great for the lift force of the fluid acting on the cylinders.

6.3 Design Concepts

This section outlines a few conceptual designs. The part views in Figure 37 show the slider concept design.

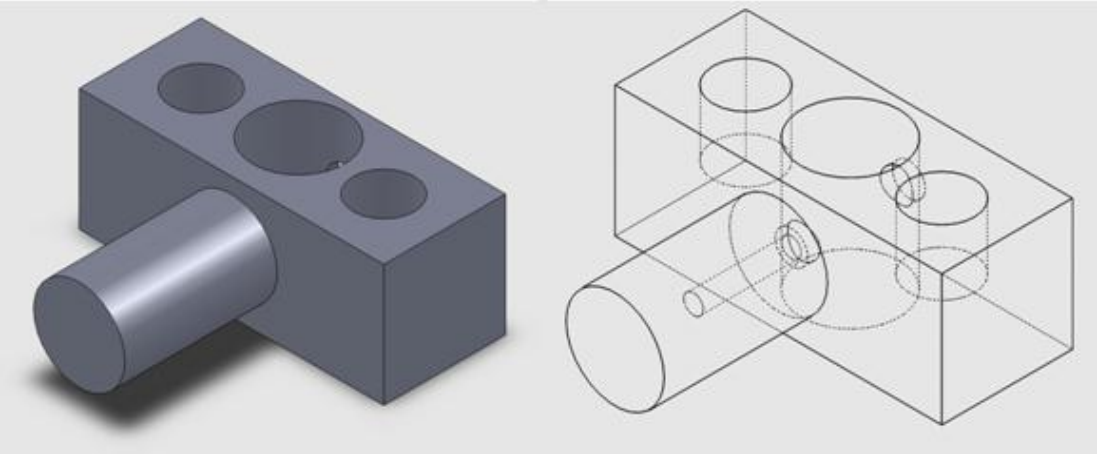

Figure 37: Slider Concept Design

In this design, the large center hole is to hold a linear bearing. The two adjacent holes provide a location to secure the ends of a spring and a damper. The circular protrusion will be secured to the block by a bolt. The bolt hole in the block will be counter bored, as shown in Figure 38 below.

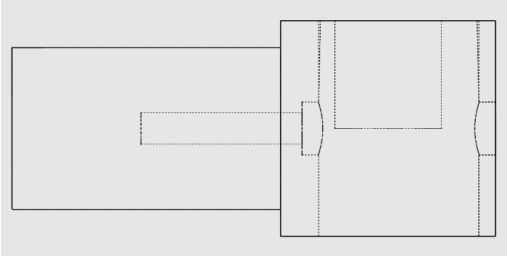

Figure 38: Right View of Slider Concept

The circular protrusion will be inserted into a hole in the end of a cylinder for a firm fit. For tests with aluminum pipes, this protrusion can be bolted into the appropriate sized end caps pressed onto either side of the cylinder. The guides for the linear bearings will be attached to a stationary frame. This frame will need to be secured within the testing cross section. This frame will hold a LVDT sensor above the cylinder. The core of the LVDT will be attached directly to the cylinder so that it will move in conjunction with the displacement of the cylinder.

6.4 Suggested Experiments

As previously discussed, testing facilities such as those at Alden Labs would increase the flexibility of future experiments. Based on the new testing rig, a series of new experiments are proposed below. These values are based on the mathematical model discussed in Chapter 3. In addition to allowing for a test rig with much higher values of damping, the new facilities will allow for tests that occur both outside and within the lock-in ranges. A much greater range of Reynolds numbers can also be achieved to further develop the relationship between flow conditions and power.

Experiment 1

The length of the cylinder is a constant length of 1m and the damping will have a constant value. A range of cylinder diameters are chosen to achieve aspect ratios from 1:6 to 1:10. The stiffness of each setup is chosen so that a 1:1 ratio of vortex shedding frequency to natural frequency will occur at an approximate flow speed of 1.5 m/s. The natural frequency calculation uses the mass of the cylinder with the hydrodynamic mass and the mass of the rest of the test rig. The test rig is assumed to have a mass of 10kg, its maximum based on the task specifications. With flow speeds of approximately below 1 m/s or above 1.8m/s, the system will be outside of the theoretical +/-30% lock-in region. For each cylinder, the flow velocity will be adjusted at constant intervals from 0m/s to 2m/s. At each interval, the displacement of the cylinder will be recorded for 60 seconds. This will allow for data that will show the difference in amplitude, frequency, power, and efficiency of the cylinder within the lock-in range and outside of the lock-in range. By comparing these same results between the varying cylinders, the relationship between aspect ratio and efficiency can be further explored. Additionally, these results can be used to create a non-dimensional curve to plot the relationship between the power coefficient and the Reynolds Number. This experiment can be repeated with different stiffness values to create a different natural frequency for each of the cylinders tested. Additional cylinder sizes could also be used.

Table 9: Proposed Setups for Testing the Lock-in Range

Aspect Ratio	Diameter	Cylinder Mass	Stiffness
1:6	6in/0.15m	4.1kg	4000N/m
1:7	5in/0.13m	3.4kg	4500N/m
1:8	4.5in/0.11m	3.0kg	5000N/m
1:9	4in/0.10m	2.7kg	6000N/m
1:10	3in/0.90m	2.3kg	7000N/m

Experiment 2

This experiment will explore the relationship between damping and the oscillations of the cylinders. The same cylinders and same values of stiffness from the previous experiment can be used. The velocity for each test is held constant at 1m/s so that the cylinders will oscillate within the lock-in region. The damping ratio of the cylinders will be adjusted at constant intervals between the minimum value and the maximum value achievable by the test setup. For each damping ratio, the displacement of the cylinder will be recorded for 60 seconds. These tests will show the relationship between the damping of the system and the ability of the system to oscillate. The objective of this portion of the testing schedule is to determine what the ideal value of zeta is, or at what value the most power can be extracted from the cylinder without critically interfering with cylinder oscillations.

7 Conclusions

Through mathematical modeling and small-scale experiments, the potential for vortex-induced vibrations as an energy source was studied. Initial research was conducted on VIV theory and existing aquatic energy technologies, including VIVACE. Based on the background research, a mathematical model was created in order to predict the relationship between experimental parameters and cylinder response, to establish feasibility of small scale VIV testing and to create estimates for experimental results. Measured oscillation frequencies were generally in-between the measured natural frequency and the theoretically calculated shedding frequency. Because the oscillation frequencies did not match the natural frequencies, the systems were likely not fully locked- in. But because the ratio of natural frequency to oscillation frequency was consistently less than the calculated ratio of shedding frequency to the oscillation frequency, the lock-in conditions had an impact on the dynamic behavior of the cylinders. Cylinder amplitude estimates proved accurate in some cases. However, the equation for amplitude in the model is linear, whereas VIV is known to be highly non-linear.

A test set up was designed and constructed using purchased hardware, hand construction and CNC machining processes. Throughout the building and testing phases of the project, possible improvements to the set up became apparent, such as adjustable stiffness and damping. Through the use of this test set up, still water tests were conducted to measure the natural frequency of each cylinder, establish damping ratios, and to determine the hydrodynamic mass of the cylinders. Flowing water tests were then conducted to measure the displacement, velocity, and acceleration of the cylinder at various flow velocities. Tests were limited in scope, precision, and accuracy due to lack of control of flow velocity and the limited resolution of the device used to measure displacement. The motion sensor had a resolution of 1mm. This created large uncertainty for damping ratio results because the logarithmic decay was on the scale of millimeters. Because damping was a small contribution to the power equation, this did not significantly impact the uncertainty in power calculations. If future experiments were conducted with greater damping values, damping would need to be measured with higher resolution devices. The resolution of the LVDT displacement sensor would only be limited by noise in the signal conditioner and by the resolution of the output

device. This would allow for lower uncertainty values for calculated parameters such as damping. Because of the limited scope, all tests were within the lock-in range. None of the experiments were able to test the changes in oscillation behavior below or above lock-in.

The experimentally determined parameters were used with the differential equation of motion for the cylinders to calculate the force of lift with respect to time and ultimately calculate the power transferred from the fluid. From this data, a curve relating power to flow conditions was plotted and showed that the non-dimensional power term decreased logarithmically with Reynolds number. This curve could be used to predict power based on known conditions. Due to the inconsistencies between theoretical and observed added mass, this curve would only be valid for this test setup. Future experiments should continue to explore this relationship under different conditions. Additionally, the cylinder with aspect ratio of 1:8.6 showed efficiencies around 50% while the cylinder with the aspect ratio of 1:3.8 showed that the efficiency dropped to around 15%. This suggests that slender bodies will provide more efficient power extraction. However, the results showed increases in the magnitude of power with increased cylinder size. Future tests should be conducted to determine the aspect ratio that will optimize efficiency.

Overall, this project demonstrated proof of concept for scale VIV tests. At this small scale, the maximum calculated power ranged from 15 to 45 mili-watts RMS and a maximum power density of 10.3 watts/m^3. Based on lessons from this project, design of a further testing set up and a testing plan have been presented for larger scale VIV tests. The power density model showed that single cylinder power density of 60 watts per cubic meter for a 4 inch diameter, 36 inch long cylinder is feasible. These tests would allow for a greater force to overcome damping caused by a power-take off system. By incorporating a power take off system into future experiments, the validity of the analytical power calculations could be tested and true data for extractable power can be measured. Because the results showed the phenomenon occurring at flow velocities lower than the realistic conditions, the potential exists for vortex induced vibrations as a source of energy generation.

8 References

1. Bernitsas. (2009). The VIVACE Converter: Model Tests at High Damping and Reynolds Number Around 105. *Journal of Offshore Mechanics and Arctic Engineering*, 12.
2. Bernitsas, M. M., Raghavan, K., Ben-Simon, Y., & Garcia, E. M. (2008). VIVACE (Vortex Induced Vibration Aquatic Clean Energy): A New Concept in Generation of Clean and Renewable Energy From Fluid Flow. *Journal of Offshore Mechanics and Arctic Engineering*.
3. Blevins. (1990). *Flow-Induced Vibration.* New York: Van Nostrand Reinhold.
4. Govardhan, C. a. (2004). VORTEX-INDUCED VIBRATIONS. *Annual Review of Fluid Mechanics*, (p. 53).
5. MIT. (n.d.). Retrieved 10 2010, from Open Course Ware.
6. Raghavan, K., Bernitsas, M. M., & Maroulis, D. E. (2009). Effect of Bottom Boundary on VIV for Energy Harnessing at 8E3<Re<1.5E5. *Journal of Offshore Mechanics and Arctic Engineering*.

Appendix A Still Water Decay Test Data

mass (gr)	zeta 1	zeta 2	frequency (hz)
135	0.093	0.081	1.770
135	0.128	0.046	1.900
135	0.093	0.081	1.820
135	0.128	0.046	1.860
135	0.093	0.081	1.950
mean	**0.107**	**0.067**	**1.860**
152	0.064	0.046	1.820
152	0.064	0.046	1.760
152	0.072	0.025	1.820
152	0.064	0.046	1.790
152	0.072	0.025	1.820
mean	**0.067**	**0.038**	**1.802**

Table 10: Data Summary of 0.75" Cylinder

mass (gr)	zeta 1	zeta 2	frequency (hz)
155	0.077	0.046	1.600
155	0.064	0.046	1.589
155	0.077	0.046	1.600
155	0.058	0.064	1.600
155	0.058	0.064	1.600
mean	**0.067**	**0.053**	**1.598**
172	0.070	0.064	1.589
172	0.058	0.064	1.579
172	0.058	0.064	1.589
172	0.070	0.064	1.579
172	0.077	0.046	1.600
mean	**0.067**	**0.061**	**1.587**

Table 11: Data Summary of 1" Cylinder

mass (gr)	zeta 1	zeta 2	frequency (hz)
272	0.046	0.029	1.170
272	0.055	0.014	1.180
272	0.075	reject	1.180
272	0.060	0.015	reject
272	0.064	0.017	1.150
mean	**0.060**	**0.019**	**1.170**
289	0.055	0.014	1.140
289	0.055	0.014	1.150
289	0.055	0.014	1.130
289	0.043	0.027	1.130
289	0.052	0.013	1.140
mean	**0.052**	**0.016**	**1.138**

Table 12: Data Summary of 1.5" Cylinder

mass (gr)	zeta 1	zeta 2	frequency (hz)
343	0.051	0.034	0.690
343	0.053	0.026	0.690
343	0.053	0.035	0.690
343	0.053	0.035	0.680
343	0.051	0.043	0.690
mean	**0.052**	**0.035**	**0.688**
377	0.041	0.031	0.678
377	0.058	0.029	0.678
377	0.048	0.031	0.678
377	0.055	0.031	0.690
377	0.048	0.031	0.690
mean	**0.050**	**0.031**	**0.683**

Table 13: Data Summary of 2" Cylinder

Appendix B Flowing Water Test Data

Tables 14: 0.75" Cylinder Final Data

trial	1	2	3	4
m cyl (kg)	0.104	0.121	0.138	0.155
m tot (kg)	0.317	0.334	0.351	0.374
m*	0.488	0.568	0.648	0.708
d (m)	0.0267	0.0267	0.0267	0.0267
k (N/m)	47.6	47.6	47.6	47.6
Zeta	0.11	0.11	0.11	0.11
fn water (hz)	1.950	1.900	1.860	1.802
L (m)	0.22	0.22	0.22	0.22

Trial 1

mean flow(m/s)	SD %	f shd (hz)	f osc (hz)	osc/shd	f*	X mean (m)	Prms (W)	U*	η	Cp	Re	A/D
0.250	7.0	1.850	1.919	1.037	0.984	0.013	0.0169	4.791	0.37	0.37	5.09E+03	0.49
0.246	6.8	1.822	1.978	1.085	1.014	0.016	0.0213	4.718	0.49	0.49	5.01E+03	0.60
0.251	6.6	1.862	1.963	1.054	1.006	0.016	0.0213	4.822	0.46	0.46	5.12E+03	0.60
0.273	9.7	2.022	2.095	1.036	1.074	0.018	0.0272	5.235	0.46	0.46	5.56E+03	0.67
0.301	5.8	2.234	2.124	0.951	1.089	0.018	0.0302	5.784	0.38	0.38	6.14E+03	0.67
mean	**7.2**								**0.43**	**0.43**		**0.61**

Trial 2

mean flow(m/s)	SD %	f shd (hz)	f osc (hz)	osc/shd	f*	X mean (m)	Prms (W)	U*	η	Cp	Re	A/D
0.243	6.5	1.805	1.904	1.055	1.002	0.013	0.0186	4.798	0.44	0.44	4.96E+03	0.49
0.265	7.8	1.964	1.919	0.977	1.010	0.016	0.0221	5.222	0.41	0.41	5.40E+03	0.60
0.242	6.6	1.794	1.934	1.078	1.018	0.016	0.0216	4.768	0.52	0.52	4.93E+03	0.60
0.253	7.2	1.874	1.978	1.055	1.041	0.017	0.0244	4.981	0.52	0.52	5.15E+03	0.64
0.293	6.6	2.172	2.036	0.937	1.072	0.018	0.0285	5.774	0.39	0.39	5.97E+03	0.67
mean	**6.9**								**0.45**	**0.45**		**0.60**

Trial 3

mean flow(m/s)	SD %	f shd (hz)	f osc (hz)	osc/shd	f*	X mean (m)	Prms (W)	U*	η	Cp	Re	A/D
0.240	6.7	1.778	1.885	1.060	1.013	0.015	0.0193	4.829	0.48	0.48	4.89E+03	0.56
0.240	10.0	1.776	1.875	1.056	1.008	0.016	0.0213	4.823	0.53	0.53	4.88E+03	0.60
0.264	8.6	1.954	1.943	0.995	1.045	0.017	0.0229	5.306	0.43	0.43	5.37E+03	0.64
0.266	8.6	1.973	1.973	1.000	1.061	0.017	0.0246	5.356	0.45	0.45	5.42E+03	0.64
0.281	8.5	2.084	2.041	0.979	1.097	0.018	0.0277	5.658	0.43	0.43	5.73E+03	0.67
mean	**8.5**								**0.46**	**0.46**		**0.62**

Trial 4

mean flow(m/s)	SD %	f shd (hz)	f osc (hz)	osc/shd	f*	X mean (m)	Prms (W)	U*	η	Cp	Re	A/D
0.246	8.5	1.823	1.865	1.023	1.035	0.016	0.0201	5.109	0.46	0.46	5.01E+03	0.60
0.247	5.5	1.832	1.875	1.024	1.041	0.017	0.022	5.134	0.50	0.50	5.03E+03	0.64
0.240	6.6	1.781	1.885	1.058	1.046	0.016	0.0214	4.992	0.53	0.53	4.90E+03	0.60
0.277	5.2	2.056	1.943	0.945	1.078	0.017	0.0247	5.761	0.40	0.40	5.65E+03	0.64
0.296	5.0	2.193	2.002	0.913	1.111	0.018	0.0265	6.146	0.35	0.35	6.03E+03	0.67
mean	**6.2**								**0.45**	**0.45**		**0.63**

Tables 15: 1" Cylinder final Data

trial	1	2	3	4
m cyl (kg)	0.158	0.175	0.192	0.209
m tot (kg)	0.475	0.482	0.502	0.519
m*	0.498	0.571	0.619	0.674
d (m)	0.0334	0.0334	0.0334	0.0334
k (N/m)	47.6	47.6	47.6	47.6
Zeta	0.067	0.067	0.067	0.067
fn water (hz)	1.60	1.59	1.55	1.52
L (m)	0.22	0.22	0.22	0.22

Trial 1

mean flow(m/s)	SD %	f shd (hz)	f osc (hz)	osc/shd	f*	X mean (m)	Prms (W)	U*	η	Cp	Re	A/D
0.247	8.9	1.462	1.631	1.115	1.021	0.011	0.0176	4.622	0.32	0.32	6.29E+03	0.33
0.256	9.7	1.516	1.553	1.024	0.972	0.014	0.0158	4.793	0.26	0.26	6.52E+03	0.42
0.258	7.6	1.531	1.699	1.110	1.063	0.018	0.0199	4.838	0.32	0.32	6.58E+03	0.54
0.272	8.8	1.614	1.690	1.047	1.057	0.019	0.0202	5.100	0.27	0.27	6.94E+03	0.57
0.293	6.6	1.737	1.709	0.984	1.069	0.020	0.0207	5.490	0.22	0.22	7.47E+03	0.60
mean	**8.3**								**0.28**	**0.28**		**0.49**

Trial 2

mean flow(m/s)	SD %	f shd (hz)	f osc (hz)	osc/shd	f*	X mean (m)	Prms (W)	U*	η	Cp	Re	A/D
0.237	7.6	1.403	1.514	1.079	0.954	0.011	0.0154	4.466	0.32	0.32	6.03E+03	0.31
0.238	6.2	1.410	1.572	1.115	0.991	0.018	0.0199	4.486	0.40	0.40	6.06E+03	0.52
0.261	6.7	1.549	1.611	1.040	1.015	0.020	0.0226	4.930	0.35	0.35	6.66E+03	0.60
0.274	5.6	1.625	1.650	1.015	1.040	0.022	0.0252	5.173	0.33	0.33	6.99E+03	0.66
0.282	3.9	1.669	1.680	1.006	1.058	0.022	0.0247	5.313	0.30	0.30	7.18E+03	0.66
mean	**6.0**								**0.34**	**0.34**		**0.55**

Trial 3

mean flow(m/s)	SD %	f shd (hz)	f osc (hz)	osc/shd	f*	X mean (m)	Prms (W)	U*	η	Cp	Re	A/D
0.223	8.8	1.323	1.494	1.129	0.964	0.015	0.0144	4.312	0.35	0.35	5.69E+03	0.45
0.251	8.1	1.489	1.543	1.037	0.996	0.018	0.0194	4.851	0.33	0.33	6.40E+03	0.54
0.262	6.2	1.554	1.611	1.037	1.040		0.0241	5.065	0.36	0.36	6.69E+03	0.00
0.270	8.8	1.600	1.611	1.007	1.040	0.021	0.0233	5.214	0.32	0.32	6.88E+03	0.63
0.284	6.6	1.681	1.641	0.976	1.059	0.023	0.025	5.477	0.30	0.30	7.23E+03	0.69
mean	**7.7**								**0.33**	**0.33**		**0.46**

Trial 4

mean flow(m/s)	SD %	f shd (hz)	f osc (hz)	osc/shd	f*	X mean (m)	Prms (W)	U*	η	Cp	Re	A/D
0.221	9.5	1.312	1.484	1.131	0.974	0.016	0.015	4.347	0.38	0.38	5.64E+03	0.48
0.240	8.5	1.422	1.514	1.064	0.993	0.018	0.0193	4.712	0.38	0.38	6.12E+03	0.54
0.255	8.8	1.509	1.572	1.042	1.032	0.022	0.0223	4.999	0.37	0.37	6.49E+03	0.66
0.281	5.7	1.666	1.621	0.973	1.064	0.023	0.0257	5.520	0.32	0.32	7.16E+03	0.69
0.285	5.8	1.691	1.631	0.965	1.070	0.024	0.0274	5.602	0.32	0.32	7.27E+03	0.72
mean	**7.7**								**0.35**	**0.35**		**0.62**

Tables 16: 1.5" Cylinder final Data

trial	1	2	3
m cyl (kg)	0.272	0.306	0.340
m tot (kg)	0.881	0.915	0.949
m*	0.447	0.502	0.558
d (m)	0.0483	0.0483	0.0483
k (N/m)	47.6	47.6	47.6
Zeta	0.06	0.06	0.06
fn water (hz)	1.17	1.15	1.13
L (m)	0.22	0.22	0.22

Trial 1

mean flow(m/s)	SD %	f shd (hz)	f osc (hz)	osc/shd	f*	X mean (m)	Prms (W)	U*	η	Cp	Re	A/D
0.279	6.5	1.144	1.094	1.046	0.935	0.014	0.0142	4.939	0.12	0.12	1.03E+04	0.30
0.301	9.4	1.235	1.123	1.099	0.960	0.015	0.0162	5.330	0.11	0.11	1.11E+04	0.31
0.304	5.8	1.245	1.104	1.128	0.943	0.019	0.0171	5.374	0.12	0.12	1.12E+04	0.39
0.335	4.9	1.373	1.191	1.153	1.018	0.020	0.019	5.928	0.10	0.10	1.24E+04	0.41
0.366	4.6	1.501	1.338	1.122	1.143	0.024	0.0326	6.480	0.13	0.13	1.35E+04	0.50
mean	**6.2**								**0.11**	**0.11**		**0.38**

Trial 2

mean flow(m/s)	SD %	f shd (hz)	f osc (hz)	osc/shd	f*	X mean (m)	Prms (W)	U*	η	Cp	Re	A/D
0.239	7.6	0.980	1.084	0.904	0.944	0.014	0.0129	4.311	0.18	0.18	8.81E+03	0.29
0.238	10.4	0.976	1.094	0.892	0.953	0.016	0.0142	4.293	0.20	0.20	8.78E+03	0.33
0.262	11.1	1.074	1.123	0.956	0.978	0.018	0.0161	4.725	0.17	0.17	9.66E+03	0.37
0.273	10.7	1.119	1.231	0.909	1.072	0.019	0.0207	4.924	0.19	0.19	1.01E+04	0.39
0.308	6.5	1.263	1.24	1.018	1.080	0.02	0.0247	5.555	0.16	0.16	1.14E+04	0.41
mean	**9.3**								**0.18**	**0.18**		**0.36**

Trial 3

mean flow(m/s)	SD %	f shd (hz)	f osc (hz)	osc/shd	f*	X mean (m)	Prms (W)	U*	η	Cp	Re	A/D
0.230	11.7	0.941	1.084	0.868	0.962	0.015	0.0118	4.215	0.18	0.18	8.46E+03	0.31
0.230	10.5	0.942	1.084	0.869	0.962	0.017	0.0141	4.221	0.22	0.22	8.47E+03	0.35
0.269	7.0	1.102	1.104	0.998	0.979	0.018	0.0145	4.937	0.14	0.14	9.91E+03	0.37
0.248	8.7	1.017	1.094	0.930	0.970	0.015	0.0153	4.557	0.19	0.19	9.15E+03	0.31
0.294	8.8	1.204	1.211	0.994	1.074	0.02	0.0192	5.393	0.14	0.14	1.08E+04	0.41
mean	**9.3**								**0.18**	**0.18**		**0.35**

Tables 17: 2" Cylinder final Data

trial	1	2
m cyl (kg)	0.337	0.405
m tot (kg)	1.267	1.335
m*	0.362	0.435
d (m)	0.060	0.060
k (N/m)	23.8	23.8
Zeta	0.052	0.052
fn water (hz)	0.688	0.672
L (m)	0.22	0.22

Trial 1

mean flow(m/s)	SD %	f shd (hz)	f osc (hz)	osc/shd	f*	X mean (m)	Prms (W)	U*	η	Cp	Re	A/D
0.215	12.1	0.704	0.752	0.937	1.093	0.036	0.0247	5.170	0.38	0.38	9.87E+03	0.60
0.247	9.6	0.811	0.791	1.025	1.150	0.039	0.0317	5.951	0.32	0.32	1.14E+04	0.65
0.272	9.3	0.894	0.830	1.078	1.207	0.033	0.0395	6.566	0.30	0.30	1.25E+04	0.55
0.320	5.4	1.049	0.879	1.194	1.277	0.037	0.0496	7.704	0.23	0.23	1.47E+04	0.61
0.327	6.8	1.073	0.889	1.208	1.292	0.040	0.0613	7.880	0.27	0.27	1.50E+04	0.66
mean	**8.6**								**0.30**	**0.30**		**0.61**

Trial 2

mean flow(m/s)	SD %	f shd (hz)	f osc (hz)	osc/shd	f*	X mean (m)	Prms (W)	U*	η	Cp	Re	A/D
0.207	12.3	0.679	0.713	0.952	1.061	0.035	0.0164	5.101	0.28	0.28	9.51E+03	0.58
0.220	10.1	0.722	0.732	0.986	1.089	0.035	0.0197	5.424	0.28	0.28	1.01E+04	0.58
0.259	10.0	0.850	0.772	1.102	1.149	0.038	0.0309	6.392	0.27	0.27	1.19E+04	0.63
0.277	8.0	0.909	0.781	1.164	1.163	0.037	0.0317	6.833	0.23	0.23	1.27E+04	0.61
0.319	9.3	1.047	0.830	1.262	1.235	0.037	0.0436	7.872	0.20	0.20	1.47E+04	0.61
mean	**9.9**								**0.25**	**0.25**		**0.60**